Combined Infrared Multiphoton Dissociation with Ultraviolet Photodissociation for Ubiquitin Characterization

Mohammad A Halim, Marion Girod, Luke Macaleese, Jérôme Lemoine, Rodolphe Antoine, Philippe Dugourd

Combined Infrared Multiphoton Dissociation with Ultraviolet Photodissociation for Ubiquitin Characterization

Mohammad A. Halim,[1] Marion Girod,[2] Luke MacAleese,[1] Jérôme Lemoine,[2] Rodolphe Antoine,[1] Philippe Dugourd[1]

[1]Institut Lumière Matière, Université Lyon 1 – CNRS, Université de Lyon, 69622 Villeurbanne, France

[2]Université de Lyon, Institut des Sciences Analytiques, UMR 5280, CNRS, Université Lyon 1, ENS Lyon, 69100 Villeurbanne, France

Correspondance to: Philippe Dugourd, Email : philippe.dugourd@univ-lyon1.fr

Citation: Combined Infrared Multiphoton Dissociation with Ultraviolet Photodissociation for Ubiquitin Characterization. M. A. Halim, M. Girod, L. MacAleese, J. Lemoine, R. Antoine and P. Dugourd. *J. Am. Soc. Mass Spectrom.* (2016). http://dx.doi.org/10.1007/s13361-016-1419-8

Graphical Abstract

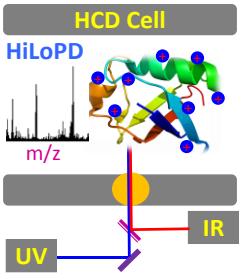

Abstract. Herein we report the successful implementation of the consecutive and simultaneous photodissociation with high (213 nm) and low (10.6 μm) energy photons (HiLoPD, high-low photodissociation) on ubiquitin in a Quadrupole-Orbitrap mass spectrometer. Absorption of high-energy UV photon is dispersed over the whole protein and stimulates extensive C-C_α backbone fragmentation while low-energy IR photons gradually increases the internal energy and thus preferentially dissociates the most labile amide (C-N) bonds. We noticed that simultaneous irradiation of UV and IR lasers on intact ubiquitin in a single MS/MS experiment provides a rich and well-balanced fragmentation array of a/x, b/y and z ions. Moreover, secondary fragmentation from a/x and z ions leads to the formation of satellite side-chain ions (d, v and w) and can help to distinguish isomeric residues in a protein. Implementation of high-low photodissociation in a high-resolution mass spectrometer may offer considerable benefits to promote a comprehensive portrait of protein characterization.

Keywords: Photodissociation; UVPD; IRMPD; Ubiquitin; Top-down Proteomics;

Introduction

Photon-based activation methods including ultraviolet photodissociation (UVPD) [1–3] and infrared multiphoton dissociation (IRMPD)[4–6] have received great attention as an alternative to electron-driven methods [7–11]. In recent years, UVPD has been implemented in high resolution mass spectrometry and employed for peptide and whole protein characterizations [12–19]. High energy UV photons preferentially cleave C_{α}–C bond in peptides and proteins producing abundant a/x ions. Other fragment ions such as c/z, and y ions are also detected in UVPD providing nearly complete sequence coverages [12, 20].

Contrasting to UVPD and electron transfer dissociation (ETD), multiple low energy IR photon excitation selectively breaks the most labile amide (C-N) bonds and generates b and y ions similar to the traditional slow-heating collision activation dissociation (CAD) method [21]. IRMPD has been implemented in different instruments including quadrupole ion traps [22] and dual pressure linear ion traps [6, 23, 24]. Vasicek *et al* reported the execution of IRMPD in the HCD (High Collision Dissociation) cell of a modified hybrid linear ion trap-Orbitrap mass spectrometer [25].

The dissociation mechanisms involved after high and low energy photon excitations are quite different. Absorption of a single high energy photon (in the UV) is sufficient to induce dissociation of a peptide and protein in gas phase. On the other hand, multiple absorption of low energy photons (in the IR) are required before fragmentation. Excitation is followed by fast internal vibrational redistribution (IVR) and causes a slow and steady rise of the internal energy until it exceeds the dissociation threshold and thus induces cleavage of the labile bonds [2].

Despite some analytical challenges, coupling of high and low energy activation pathways in a single MS/MS event is expected to offer diverse fragmentation arrays and thus deliver improved,

efficient, and well-balanced fragmentation for whole protein characterization. Tsybin *et al* reported the implementation of IRMPD with electron capture dissociation (ECD) in FT-ICR mass spectrometer [26]. Electron and photon irradiation significantly improved the formation of sequence ions for peptides and proteins. Simultaneous IR photoactivation with ETD, known as activated ion electron transfer dissociation (AI–ETD), is also implemented in an ion trap-Orbitrap Elite system [27]. Moreover, tandem ETD spectra exhibited abundant peaks related to unreacted and charge reduced precursors. Hybrid AI-ETD showed better performance for lower charge states and produce specific fragment ions. The combination of UVPD with ETD (known as ETUVPD) in an ion trap-Orbitrap has also been reported [28]. The combined ETUVPD method showed balanced fragment ions with increased number of c and z ions. The fragmentation efficiency of ETD can also be enhanced by other means such as additional activation with CID and HCD, known as ETciD and EThcd [29,30]. These hybrid methods showed rich fragmentation spectra compared to CID, HCD and ETD alone.

Although a few studies are coupling electron and photon based methods, integrating electron-driven technique with low or high collision activation approaches, so far there is no study reporting the combination of high and low energy photons for characterizing protein within a single MS/MS framework. Here, we report the implementation of a method combining solid-state 5th harmonic 213 nm laser excitation with 10.6 μm CO_2 laser excitation in hybrid quadrupole-Orbitrap mass spectrometer using different excitation schemes (consecutive IR+UV, UV+IR and simultaneous UV/IR) for top-down characterization of ubiquitin. This high-low energy photon based method (HiLoPD) improves the fragmentation pattern providing well-proportioned a/x, b/y and z-ions with richness of secondary fragment ions including d, v and w.

Materials and Methods

Laser setup and experiments. A simple schematic presentation of the execution of combined IRMPD and UVPD irradiation in the HCD cell of a hybrid quadrupole-Orbitrap is presented in **Figure 1**. IRMPD experiments were performed using a 50 W cw-CO_2 laser (ULR-50, Universal Laser System®, Scottsdale, AZ). The wavelength of the CO_2 laser is 10.6 μm with a beam diameter and divergence (full angle) of 4±1 mm and 5±1 mrad, respectively. 60% of the nominal laser power was used. The IR beam is directed to the HCD cell using gold mirrors. The IR beam was gated on an external TTL signal. Irradiation times from 0.1 to 1 s were tested. The N_2 pressure in the HCD cell was adjusted to optimize the IR fragmentation while avoiding significant loss of signal (pressure controller set to ~0.09 MPa). For the UVPD experiments, the fifth harmonic (λ=213 nm, ~1 mJ/pulse) of a 20 Hz BrillantB solid-state Nd:YAG laser (Quantel, Les Ulis, France) was used. A mechanical shutter (SH05/TSC001, Thorslab) was used to allow, on demand, the beam in the HCD cell. For UVPD, the optimal shutter open time was determined to be 0.2 s (4 laser shots) was determined. In order to combine both CO_2 and UV laser beams, a half-moon gold mirror was used on the IR beam path to the HCD cell. Also, a BaF_2 window (wavelength range 0.2-12 μm, Ø 25.4 mm, thickness 5 mm) was placed at the rear of the HCD cell, which transmit both IR (10.6 μm) and UV (213 nm) beams with 90 and 85% efficiency, respectively.

In order to irradiate ions only when they are in the HCD cell, the voltage on test-point 18 (TP18), located on Q-Exactive electronic board, was monitored. In our experimental conditions, the falling edge (-10 V $\rightarrow$ -350 V) on the TP18 is used to determine the moment when ions are ejected from the C-trap to the HCD-cell (see **Figure S1**). Two independent TTL pulses are then generated, with width and delay adjustable with regards to the TP18 trigger. The TTL pulses are used to lift the gate on the CO_2 laser and open the shutter on the UV beam path.

Three different coupling schemes between IR and UV were implemented (**Figure S1**). In scheme I, CO_2 laser was *ON* for 1 s and then followed by 4 UV pulses (0.2 s). In scheme II, 4 pulses of UV were admitted in the HCD cell first, and followed by 1 s of CO_2 laser. In those first two schemes, IR and UV were used consecutively: when CO_2 laser was *ON*, the UV laser was *OFF* and *vice versa*. In scheme III, the CO_2 laser was turned *ON* and the UV shutter was open concomitantly. As in previous schemes, IR was left *ON* for 1 s while the UV shutter was left open for 0.2 s (4 pulses). In each scheme, the coupled IR/UV irradiation takes place during single HCD events in MS^2 sequences.

Mass Spectrometry. All experiments were performed on a hybrid quadrupole-Orbitrap Q-Exactive® mass spectrometer (Thermo Fisher Scientific, San Jose, CA, USA) equipped with a HESI ion source. Ubiquitin (76 residues, 8.6 kDa) from bovine erythrocytes was obtained from Sigma-Aldrich and used without any further purification. Ubiquitin samples were prepared at 10 μM concentration in 50/49/1 (v/v/v) methanol/water/acetic acid and directly infused to MS at a flow rate of 5 μL/min. All mass spectra were acquired using a mass range of 200-2000 *m/z* and resolving power of 140000 at *m/z* 400. The AGC (Automatic Gain Control) target was set to $5x10^6$ and the maximum injection time was set at 250 ms. The isolation width was 8-10 Th. To avoid collisions and CID contamination, HCD collision energy was set to the minimum 2 eV. All experiments were performed for 3 microscans and averaging for 50 scans.

Data Analysis. Raw files were deconvoluted and deisotoped to the neutral monoisotopic masses using Xtract algorithm provided by Thermo Scientific Inc. Manual analysis of IRMPD, UVPD, and combined UVPD and IRMPD data was performed with the aid of ProSight Light software [31] and Protein Prospector V5.14.4. (http://prospector.ucsf.edu/prospector/mshome.htm). All major ion types (a, a+1, a+2, b-1, b, b+1, b+2, c-1, c, c+1, x-1, x, x+1, x+2, y, y-1, y-2, z-1, z, z+1) were

considered. We observed substantial number of secondary fragment ions including d, v and w which were analyzed by Protein Prospector. H_2O and NH_3 losses from the fragment ions were also considered. Single protein mode with a fragment mass tolerance set to 15 ppm was used for all methods.

Results and Discussion

Optimization of IRMPD on Intact Protein. The overall performance of IRMPD is hindered by the failure to provide adequate fragmentation of peptide or proteins at the standard pressure in the HCD cell. Although relatively high pressure is desirable for collision cooling during the ion accumulation to obtain maximum trapping efficiency, it is disadvantageous to ion activation and dissociation [32]. In the Q-Exactive mass spectrometer, the HCD cell and C-trap are filled with N_2 gas with chamber pressure of ~10^{-5} mbar known as High Vacuum (HV) region whereas Orbitrap kept the low pressure at ~10^{-10} mbar designated as Ultra High Vacuum (UHV) region. A pressure regulator allows control of the collision gas valve and hence the pressure in the HCD cell. The position of the pressure controller also has an effect on the High Vacuum pressure value. Here, where we discuss high and low pressure it is the HCD cell pressure governed by the pressure controller position and estimated *via* High Vacuum gauge that is being considered. A previous study on hybrid QLT-Orbitrap indicated that the level of the collision gas (N_2) must be lowered [33]. At high pressure in the chamber (HV ~4.6 x 10^{-5} mbar, pressure controller 0.5 MPa), there is no noticeable photodissociation observed for +12 charge state ion of ubiquitin even at longer (1 s) irradiation time (**Figure 2)**. The collision frequency, which is associated with the collision cross-section [34] of the protein, of +12 charge state ion of ubiquitin is typically around 6700 s^{-1} at high pressure of 10^{-4} mbar (**Figure S2**). This high collision rate promotes collision deactivation and

cooling of the protein before it can undergo fragmentation, resulting in limited photodissociation being observed. The fragmentation efficiency improves as the pressure is reduced. At low pressure (HV ~9.3 x 10^{-6} mbar, pressure controller ~0.09 MPa), the dissociation efficiency is augmented significantly for +12 charged precursor ion of ubiquitin. At ~9.3 x 10^{-6} mbar pressure, the collision frequency of +12 ion of ubiquitin is reduced. It is noticed that pressure lower than ~0.09 MPa on the pressure controller can lead to more fragment ions, however, the signal is not very stable at this range and moreover sensitivity and resolution are also decreased. The irradiation time also has a major impact on the photodissociation yield of ubiquitin (**Figure S3**). At lower pressure, when ubiquitin is irradiated for 0.1 s, the fragmentation efficiency is only about 25% which is considerably improved to 68% for 1 s irradiation time **(Figure S4**). Most previous studies related to IRMPD used a laser irradiation time less than 0.1 s in LIT [6 , 27]. As is evident from other studies, higher laser power is required for superior fragmentation efficiency of larger peptides and intact proteins [6,35,33,36].

The IRMPD on the +12 charge state ion of ubiquitin identifies a total of 141 fragment ions of which 41 are b-type and 98 are y-type ions. Exact masses and assignments of the ions detected in the IRMPD of the 12+ precursor ion (*m/z*=714.7279) of ubiquitin are summarized in **Table S1**. For this charge state, more than double the number of y-type ions are identified as compared to b-type ions. The sequence coverage for the +12 ion is 59% (44 bonds break) which is significantly higher than the coverage 24% (18 bonds break) reported earlier when IRMPD was first implemented in high resolution Orbitrap mass spectrometer (**Figure S5**) [25]. We notice that 60% of the nominal laser power with combination of lower pressure (HV ~9.3 x 10^{-6} mbar) and longer irradiation time (~1 s) are optimal for characterization of intact protein by IRMPD in a quadrupole-Orbitrap system.

UVPD, IRMPD and HiLoPD on Ubiquitin. The photodissociation mass spectra using IRMPD, UVPD and combined IR and UV (scheme I, II, III**)** of the +13 precursor ion of ubiquitin are presented in **Figure 3**.

First of all, the +13 precursor ion of ubiquitin was subjected to UVPD only. All 213 nm UVPD experiments have been performed in the low pressure regime (~9.3 x 10^{-6} mbar) to make unbiased comparison with consecutive or simultaneous irradiation of IRMPD and UVPD. Even at low pressure, the 213 nm UVPD on the +13 charge state ion identifies a total of 209 fragment ions (**Figure 4a**) including 68 a-type, 5 b-type, and 10 c-type ions as well as 38 x-type, 59 y-type and 28 z-type ions (**Table S2**). Along with traditional a/x, y and c/z ions, a+1/x+1, x+2, y-1, y-2, c-1, and c+1 ions of ubiquitin are also detected. Recently, we reported that the radical-driven backbone fragmentation provides 22 distinctive fragment ion types for peptide anions at 213 nm UVPD [15]. High energy UVPD (157 and 193 nm) reported abundant formation of the radical a+1 and x+1 ions [37,38,39]. Here we observed the similar feature at 213 nm (5.8 eV) UVPD which produces significant number of a+1/x+1 ion. The mechanism of the homolytic cleavage of the C_{α}-C(O) bond which produces a+1/x+1 ions has been proposed elsewhere [15]. Moreover, the formation of y-1 and y-2 occur from the secondary dissociation of the x+1 radical and is associated with presence of proline residues [38,18]. Neutral losses of NH_3 are detected from a and y ions. The UVPD sequence coverage achieved for the +13 precursor ion is 76%.

The IRMPD experiment on the +13 ion of ubiquitin detects a total of 121 fragment ions (**Figure 4a**). Exact masses and assignments of ions detected in the IRMPD of the +13 ion (*m/z*=659.8249) of ubiquitin are summarized in **Table S3**. Among them, 49 ions are b–type and 67 ions are y-type fragments. The formation of only b and y-type ions is expected from cleavages of C-N bonds proceeding *via* vibrationally-excited ground state dissociation. H_2O and NH_3 losses from the b and

y ions are also noticed, with H_2O losses being more widespread than NH_3 loss. The loss of water is energetically favorable from the protonated acidic group [40]. Ubiquitin has 7 threonine (T), 6 glutamic acid (E), 5 aspartic acid (D) and 3 serine (S) residues which may promote the widespread water loss. Low (z = +1) to high charge states (z = +12) of the b and y ions are observed, with the same fragment ion often being observed in many different charge states. For example, b_{17} ion with +2, +3, and +4 charge states are detected at *m/z* 952.5491, 635.3695, and 476.7778, respectively. The IRMPD sequence coverage of this charge state precursor ion is 44%.

The same precursor ion (z = +13) was then fragmented with UVPD in combination to IRMPD. In the consecutive scheme I, in which first IR then UV irradiation was performed, the total number of detected fragment ions is remarkably declined compared to UVPD (**Figure 4a**) alone. Despite this decrease, the number of b-type ions detected is significantly increased. The y-type ions remain same as UVPD alone. The a/x and c/z ions are also remarkably suppressed. Overall, the sequence coverage using this scheme is only 56 % (**Figure 3**). In scheme I, IR laser pulses produce ubiquitin in its vibrationally hot electronic ground state (**Figure 5a**). Excitation promotes formation of hot ions and eventually ground state dissociation. And thus less parent ions are then available for UV fragmentation. UV excitation of hot ions is also possible.

In the consecutive scheme II, when irradiation with UV laser pulses is followed by IR irradiation, the overall number of detected fragment ions is considerably higher compared to scheme I (**Figure 4a**). The number of b and y-type ions is sharply increased as compared to both UVPD and scheme I. The relaxation following electronic excitation either by light emission, internal conversion through a conical intersection or via fragmentation is expected to be fast (typically ranging from fs to ns timescales). In scheme II, IR excitation is occurring after electronic excitation and relaxation has occurred. The UV laser promotes excited states dissociation whereas IR laser subsequently

leads to the ground state dissociation (**Figure 5b**). The combination of the two dissociation mechanisms explain the large amount of detected fragment ions in scheme II. In this case, the sequence coverage for this charge state precursor ion is 71% and is comparable to the one observed in UVPD.

The simultaneous introduction of UV and IR lasers (HiLoPD, high-low photodissociation, scheme III), on the +13 ion of ubiquitin produces a more diverse range of fragment ions than any of IRMPD, UVPD, Scheme I and Scheme II (**Figure 4a**). Exact masses and assignments of the ions detected in the combined UVPD and IRMPD of the +13 ion (*m/z*=659.8249) of ubiquitin are summarized in **Table S4**. Compare to UVPD, a substantial increase in b and y ions is observed in scheme III. The number of b-type ions increases from 5 to 48 while the number of y-type ions raises from 59 to 106 ions. The number of c-type ions is increased slightly from 10 to 18. The number of x and z-type of ions remained nearly same as UVPD, whereas the number of a-type ions is decreased noticeably from 68 to 24 ions with respect to UVPD. Secondary fragmentation which leads to the formation of d, v, and w ions is also significantly increased in scheme III compared to UVPD, scheme I and II (**Figure S6**). Due to the excess energy in scheme III, elimination of other groups such as R, CO and CONH are observed near the position of primary cleavage. High energy 157 and 193 nm UVPD has also reported the side-chain losses from the a+1/x+1 ions to form d, v and w ions [39]. Kjeldsen *et al* noticed the formation of d and w ions from the Leu and Ile comprising peptide in hot electron capture dissociation [41]. Zhang and Reilly also observed the formation of v, w_a, and w_b ions from x+1 ion of Leu and Ile containing peptides by UVPD at 157 nm [42]. It is interesting to note that ubiquitin has a total of 16 Leu and Ile residues, and thus formation of these secondary ions allows to distinguish isomeric residues. In addition, HiLoPD can be applied for *de novo* sequencing of peptides [43]. The sequence coverage of the +13 ion of

ubiquitin obtained at scheme III is 83%. The photophysical interpretation of this increase in fragmentation yield is that IR irradiation concomitant to UV irradiation can lead to vibrational excitation as well as excitation of higher electronic states and thus produce a rich fragmentation array (**Figure 5c**). **Figure 6** shows the sequence maps obtained for the +13 charge state precursor ion in IRMPD, UVPD and HiLoPD (scheme III). The sequence coverage is improved in HiLoPD thanks to the combination of IR and UV irradiation. While IRMPD yields more fragment ions from the N-terminal, UVPD produces ions from the mid and C-terminal regions. Interestingly, HiLoPD able to produce fragments ions from all regions.

For a lower charge state (z = +8), the simultaneous irradiation of scheme III (HiLoPD) also showed a balanced fragmentation pattern. The total number of detected fragment ions of this charge state in scheme III is higher than both IRMPD and UVPD (**Figure 4b**) alone. A considerable number of b and y ions are observed in this lower charge state, and c-type ions are also detected. Only z-type ions remain essentially the same as in UVPD. The sequence coverage of the +8 ion of ubiquitin obtained with HiLoPD (scheme III) is 85%. Formation of d, v and w ions also is noticed for these charge states similar to +13 precursor ion.

Overall, IRMPD selectively produces b/y, and b-H_2O/y-H_2O ions whereas UVPD preferentially yields a+1/x+1, a/x, y-1, y-NH_3, z, v and w ions (**Figure S7a**). The hybrid HiLoPD (scheme III) method generates b/y, b-H_2O/y-H_2O, x, x+1, y-1, y-2, y-NH_3, z, v and w ions. Bond breaking and sequence coverage of high (z = +13) and low (z = +8) ions of ubiquitin obtained by IRMPD, UVPD and HiLoPD (scheme III) are shown in **Figure S7b and S7c**. HiLoPD allows to improve the efficiency of structural characterization of ubiquitin compared to IRMPD and UVPD. Moreover, sequence coverages obtained with HiLoPD are similar to those theoretically expected by combining UVPD and IRMPD (calculated IR+UV, see **Figure S7c**).

Conclusion

We have reported IRMPD, 213 nm UVPD, and HiLoPD patterns of ubiquitin in a hybrid quadrupole-Orbitrap mass spectrometer. Improved performance of IRMPD is observed when we use high laser powers coupled with a combination of very low pressure and longer irradiation time in the HCD cell. Significant numbers of b/y ions and neutral losses of NH_3 and H_2O are detected by IRMPD. Similar to excimer 193 nm UVPD, solid-state 213 nm UVPD can promote C_α–C cleavage generating abundant a/x, y, and z fragment ions for ubiquitin.

The Coupling of low-energy IRMPD and high-energy UVPD was implemented using three different irradiation schemes. In scheme I, where IR irradiation is followed by UV, the detected fragment ions are decreased as compared to UVPD only, which is mainly due to intense IR fragmentation prior to UV excitation. When UV irradiation was followed by IR (scheme II), the total number of detected fragment ion is slightly increased. In scheme III, while UV and IR lasers irradiation is simultaneous, the total number of detected fragment ions is increased. Excited and ground state dissociation channels promote widespread fragmentation in ubiquitin. Compared to UVPD, b/y-type ions are increased. We noticed that, while a/x fragment ions are decreasing, nearly equal number of d, v and w ions emerge, which can lead to identify the isomeric residues in a protein.

Acknowledgements

The research leading to these results has received funding from the European Research Council under the European Union's Seventh Framework Program (FP7/2007-2013 Grant agreement N°320659). We would like to thank Christian Clavier for his invaluable technical assistance. The authors like to thank Dr. Steven Daly, ILM, CNRS et Université Lyon 1, France for improving the English of this manuscript.

Supporting Information: Figure S1-S7 and Table S1-S4 are included in the supporting file.

References

1. Reilly, J.P.: Ultraviolet photofragmentation of biomolecular ions. Mass Spectrom Rev. 28, 425–447 (2009).

2. Brodbelt, J.S.: Photodissociation mass spectrometry: new tools for characterization of biological molecules. Chem. Soc. Rev. 43, 2757–83 (2014).

3. Antoine, R., Lemoine, J., Dugourd, P.: Electron photodetachment dissociation for structural characterization of synthetic and biopolymer anions. Mass Spectrom. Rev. 33, 501–522 (2014).

4. Gardner, M.W., Smith, S.I., Ledvina, A.R., Madsen, J.A., Coon, J.J., Schwartz, J.C., Stafford Jr., G.C., Brodbelt, J.S.: Infrared multiphoton dissociation of peptide cations in a dual pressure linear ion trap mass spectrometer. Anal. Chem. 81, 8109–8118 (2009).

5. Raspopov, S.A., El-Faramawy, A., Thomson, B.A., Siu, K.W.M.: Infrared multiphoton

dissociation in quadrupole time-of-flight mass spectrometry: top-down characterization of proteins. Anal. Chem. 78, 4572–7 (2006).

6. Ledvina, A.R., Lee, M.V., McAlister, G.C., Westphall, M.S., Coon, J.J.: Infrared multiphoton dissociation for quantitative shotgun proteomics. Anal. Chem. 84, 4513–4519 (2012).

7. Zhurov, K.O., Fornelli, L., Wodrich, M.D., Laskay, U.A., Tsybin, Y.O.: Principles of electron capture and transfer dissociation mass spectrometry applied to peptide and protein structure analysis. Chem. Soc. Rev. 42, 5014–5030 (2013).

8. Zubarev, R.A., Kelleher, N.L., McLafferty, F.W.: Electron capture dissociation of multiply charged protein cations. A nonergodic process. J. Am. Chem. Soc. 120, 3265–3266 (1998).

9. Syka, J.E.P., Coon, J.J., Schroeder, M.J., Shabanowitz, J., Hunt, D.F.: Peptide and protein sequence analysis by electron transfer dissociation mass spectrometry. Pro. Natl. Acad. Sci. USA. 101, 9528–9533 (2004).

10. Breuker, K., Oh, H., Lin, C., Carpenter, B.K., McLafferty, F.W.: Nonergodic and conformational control of the electron capture dissociation of protein cations. Proc. Natl. Acad. Sci. U.S.A. 101, 14011–14016 (2004).

11. Breuker, K., Oh, H., Horn, D.M., Cerda, B.A., McLafferty, F.W.: Detailed Unfolding and Folding of Gaseous Ubiquitin Ions Characterized by Electron Capture Dissociation. J. Am. Chem. Soc. 124, 6407–6420 (2002).

12. Shaw, J.B., Li, W., Holden, D.D., Zhang, Y., Griep-Raming, J., Fellers, R.T., Early, B.P., Thomas, P.M., Kelleher, N.L., Brodbelt, J.S.: Complete protein characterization using top-down mass spectrometry and ultraviolet photodissociation. J. Am. Chem. Soc. 135,

12646–12651 (2013).

13. Cannon, J.R., Cammarata, M.B., Robotham, S.A., Cotham, V.C., Shaw, J.B., Fellers, R.T., homas, P.M., Kelleher, N.L., Brodbelt, J.: Ultraviolet photodissociation for characterization of whole proteins on a chromatographic time scale. Anal. Chem. 86, 2185–2192 (2014).

14. Cammarata, M.B., Brodbelt, J.S.: Structural characterization of holo- and apo-myoglobin in the gas phase by ultraviolet photodissociation mass spectrometry. Chem. Sci. 6, 1324–1333 (2015).

15. Halim, M.A., Girod, M., MacAleese, L., Lemoine, J., Antoine, R., Dugourd, P.: 213 nm Ultraviolet Photodissociation on Peptide Anions: Radical-Directed Fragmentation Patterns. J. Am Soc. Mass Spectrom. 27, 474–486 (2016).

16. Cammarata, M.B., Thyer, R., Rosenberg, J., Ellington, A., Brodbelt, J.S.: Structural Characterization of Dihydrofolate Reductase Complexes by Top-Down Ultraviolet Photodissociation Mass Spectrometry. J. Am. Chem. Soc. 137, 9128–9135 (2015).

17. Cannon, J.R.., Martinez-Fonts, K., Robotham, S., Matouschek, A., Brodbelt, J.S.: Top-Down 193-nm Ultraviolet Photodissociation Mass Spectrometry for Simultaneous Determination of Polyubiquitin Chain Length and Topology. Anal. Chem. 87, 1812–1820 (2015).

18. Girod, M., Sanader, Z., Vojkovic, M., Antoine, R., MacAleese, L., Lemoine, J., Bonacic-Koutecky, V., Dugourd, P.: UV Photodissociation of Proline-containing Peptide Ions: Insights from Molecular Dynamics. J. Am. Soc. Mass Spctrom. 26, 432–443 (2014).

19. Fort, K.L., Dyachenko, A., Potel, C.M., Corradini, E., Marino, F., Barendregt, A.,

Makarov, A.A., Scheltema, R.A., Heck, A.J.R.: Implementation of Ultraviolet Photodissociation on a Benchtop Q Exactive Mass Spectrometer and Its Application to Phosphoproteomics. Anal. Chem. 88, 2303–2310 (2016).

20. Brodbelt, J.S.: Ion Activation Methods for Peptides and Proteins. Anal. Chem. 88, 30–51 (2016).

21. McLuckey, S.A.: Principles of collisional activation in analytical mass spectrometry. J. Am. Soc. Mass Spctrom. 3, 599–614 (1992).

22. Crowe, M.C., Brodbelt, J.S.: Infrared multiphoton dissociation (IRMPD) and collisionally activated dissociation of peptides in a quadrupole ion trap with selective IRMPD of phosphopeptides. J. Am. Chem. Soc. 15, 1581–1592 (2004).

23. Gardner, M.W., Smith, S.I., Ledvina, A.R., Madsen, J.A., Coon, J.J., Schwartz, J.C., Stafford Jr., G.C., Brodbelt, J.S.: Infrared multiphoton dissociation of peptide cations in a dual pressure linear ion trap mass spectrometer. Anal. Chem. 81, 8109–8118 (2009).

24. Madsen, J.A., Gardner, M.W., Smith, S.I., Ledvina, A.R., Coon, J.J., Schwartz, J.C., Stafford, G.C., Brodbelt, J.S.: Top-Down Protein Fragmentation by Infrared Multiphoton Dissociation in a Dual Pressure Linear Ion Trap. Anal. Chem. 81, 8677–8686 (2009).

25. Vasicek, L.A., Ledvina, A.R., Shaw, J., Griep-Raming, J., Westphall, M.S., Coon, J.J., Brodbelt, J.S.: Implementing Photodissociation in an Orbitrap Mass Spectrometer. J. Am. Soc. Mass Spctrom. 22, 1105–1108 (2011).

26. Tsybin, Y.O., Witt, M., Baykut, G., Kjeldsen, F., Håkansson, P.: Combined infrared multiphoton dissociation and electron capture dissociation with a hollow electron beam in Fourier transform ion cyclotron resonance mass spectrometry. Rapid Commun. Mass

Spectrom. 17, 1759–1768 (2003).

27. Riley, N.M., Westphall, M.S., Coon, J.J.: Activated Ion Electron Transfer Dissociation for Improved Fragmentation of Intact Proteins. Anal. Chem. 87, 7109–7116 (2015).

28. Cannon, J.R., Holden, D.D., Brodbelt, J.S.: Hybridizing Ultraviolet Photodissociation with Electron Transfer Dissociation for Intact Protein Characterization. Anal. Chem. 86, 10970–10977 (2014).

29. Swaney, D.L., McAlister, G.C., Wirtala, M., Schwartz, J.C., Syka, J.E.P., Coon, J.J.: Supplemental Activation Method for High-Efficiency Electron-Transfer Dissociation of Doubly Protonated Peptide Precursors. Anal. Chem. 79, 477–485 (2007).

30. Frese, C.K., Altelaar, A.F.M., van den Toorn, H., Nolting, D., Griep-Raming, J., Heck, A.J.R., Mohammed, S.: Toward Full Peptide Sequence Coverage by Dual Fragmentation Combining Electron-Transfer and Higher-Energy Collision Dissociation Tandem Mass Spectrometry. Anal. Chem. 84, 9668–9673 (2012).

31. Fellers, R.T., Greer, J.B., Early, B.P., Yu, X., LeDuc, R.D., Kelleher, N.L., Thomas, P.M.: ProSight Lite: Graphical software to analyze top-down mass spectrometry data. Proteomics. 15, 1235–1238 (2014).

32. Hashimoto, Y., Hasegawa, H., Waki, I.: High sensitivity and broad dynamic range infrared multiphoton dissociation for a quadrupole ion trap. Rapid. Comm. Mass Spectrom. 18, 2255–2259 (2004).

33. Ledvina, A.R., Rose, C.M., Mcalister, G.C., Syka, J.E.P., Westphall, M.S., Griep-raming, J., Schwartz, J.C., Coon, J.J.: Activated Ion ETD Performed in a Modified Collision Cell on a Hybrid QLT-Oribtrap Mass Spectrometer. J. Am. Soc. Mass Spctrom. 1623–1633

(2013).

34. Bush, M.F., Hall, Z., Giles, K., Hoyes, J., Robinson, C. V, Ruotolo, B.T.: Collision Cross Sections of Proteins and Their Complexes: A Calibration Framework and Database for Gas-Phase Structural Biology. Anal. Chem. 82, 9557–9565 (2010).

35. Brodbelt, J.S., Wilson, J.J.: Infrared multiphoton dissociation in quadrupole ion traps. Mass Spectrom. Rev. 28, 390–424 (2009).

36. Ledvina, A.R., Beauchene, N.A., McAlister, G.C., Syka, J.E.P., Schwartz, J.C., Griep-Raming, J., Westphall, M.S., Coon, J.J.: Activated-Ion Electron Transfer Dissociation Improves the Ability of Electron Transfer Dissociation to Identify Peptides in a Complex Mixture. Anal. Chem. 82, 10068–10074 (2010).

37. Zhang, L., Cui, W., Thompson, M.S., Reilly, J.P.: Structures of alpha-Type Ions Formed in the 157 nm Photodissociation of Singly-Charged Peptide Ions. J. Am. Soc. Mass Spctrom. 17, 1315–1321 (2006).

38. Madsen, J., Cheng, R.R., Kaoud, T.S., Dalby, K., Makarov, D.E., Brodbelt, J.: Charge-site-dependent dissociation of hydrogen-rich radical peptide cations upon vacuum UV photoexcitation. Chem. Eur. J. 18, 5374–5383 (2012).

39. Cui, W., Thompson, M.S., Reilly, J.P.: Pathways of peptide ion fragmentation induced by vacuum ultraviolet light. J. Am. Soc. Mass Spctrom. 16, 1384–1398 (2005).

40. Van Stipdonk, M., Kullman, M., Berden, G., Oomens, J.: IRMPD and DFT study of the loss of water from protonated 2-hydroxynicotinic acid. Int. J. Mass Spectrom. 330–332, 134–143 (2012).

41. Kjeldsen, F., Haselmann, K.F., Budnik, B.A., Jensen, F., Zubarev, R.A.: Dissociative capture of hot (3–13 eV) electrons by polypeptide polycations: an efficient process accompanied by secondary fragmentation. Chem. Phys. Lett. 356, 201–206 (2002).

42. Zhang, L., Reilly, J.P.: Peptide Photodissociation with 157 nm Light in a Commercial Tandem Time-of-Flight Mass Spectrometer. Anal. Chem. 81, 7829–7838 (2009).

43. Zhang, L., Reilly, J.P.: De Novo Sequencing of Tryptic Peptides Derived from Deinococcus radiodurans Ribosomal Proteins Using 157 nm Photodissociation MALDI TOF/TOF Mass Spectrometry. J. Proteom. Res. 9, 3025–3034 (2010).

Figures and Tables

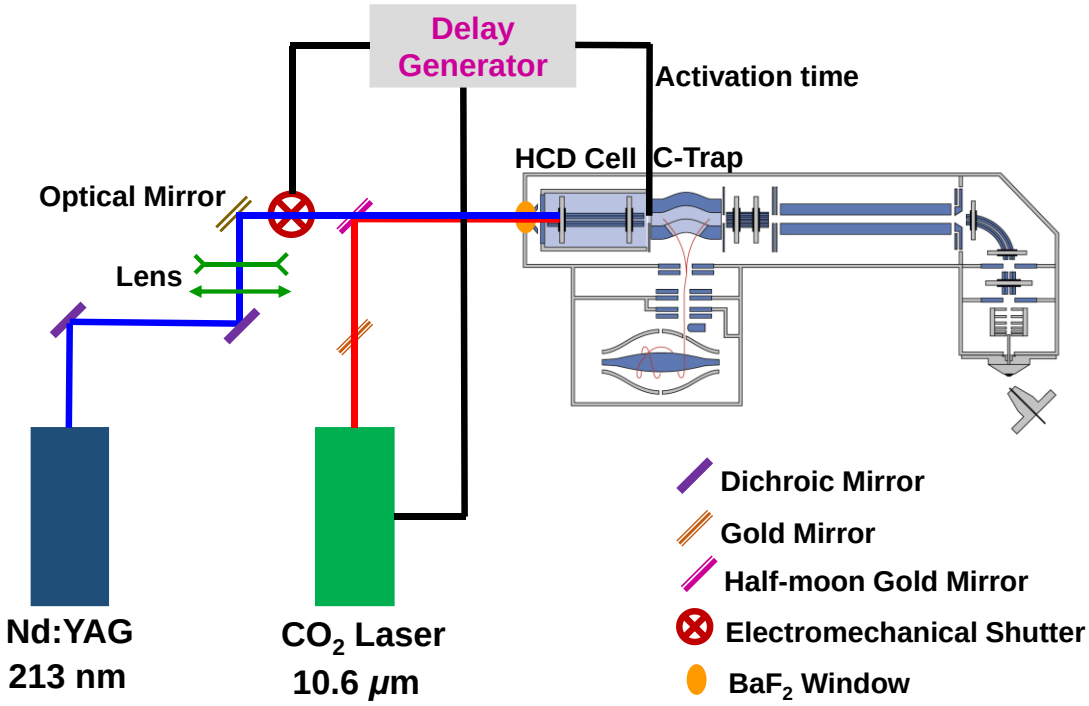

Figure 1. Schematic representation of the execution of combined IRMPD and UVPD in the HCD cell of a hybrid quadrupole-Orbitrap mass spectrometer.

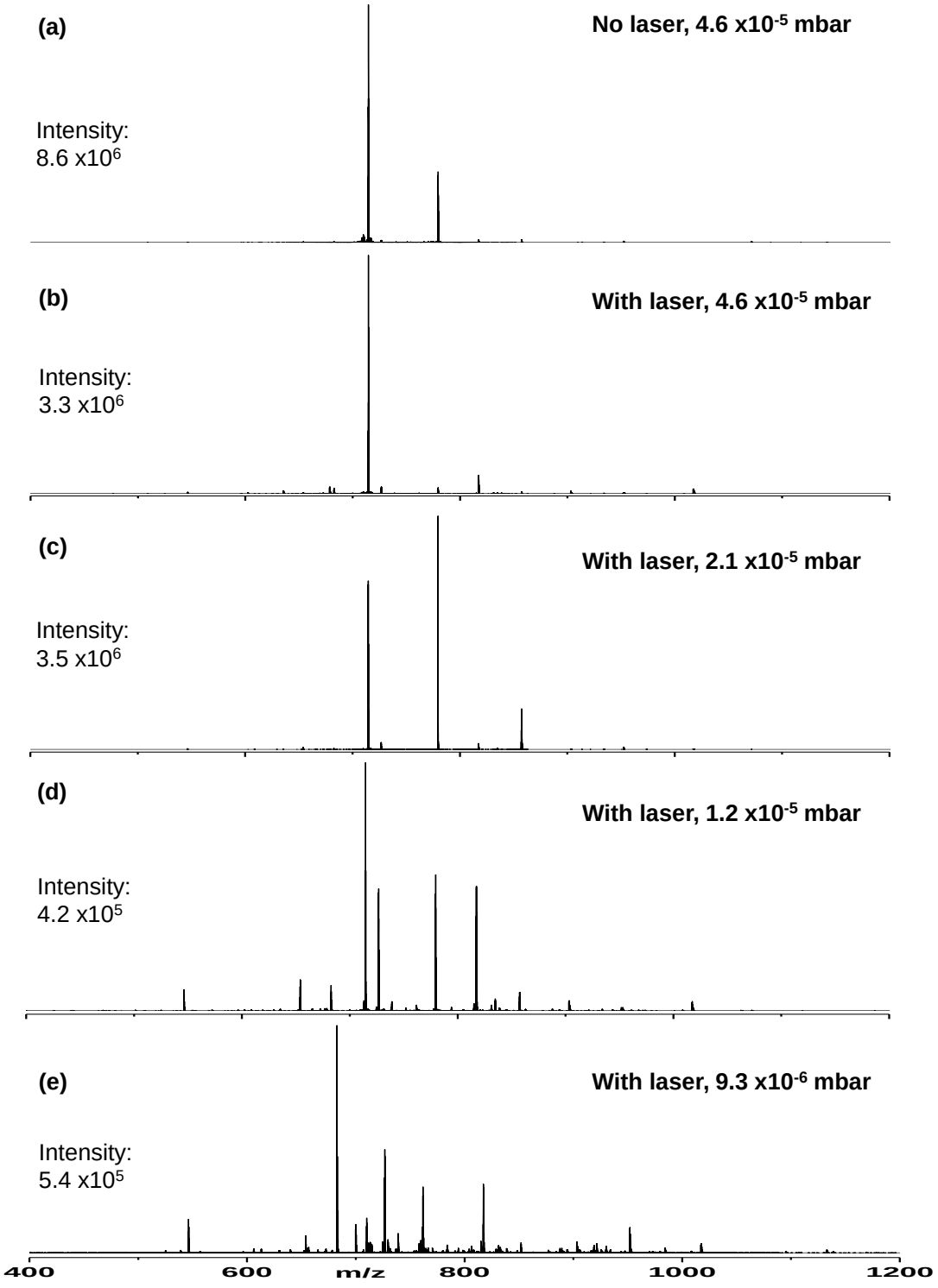

Figure 2. Impact of pressure on the fragmentation of the +12 charge state precursor ion (*m/z*=714.7279) of ubiquitin at 1 s irradiation time by IRMPD.

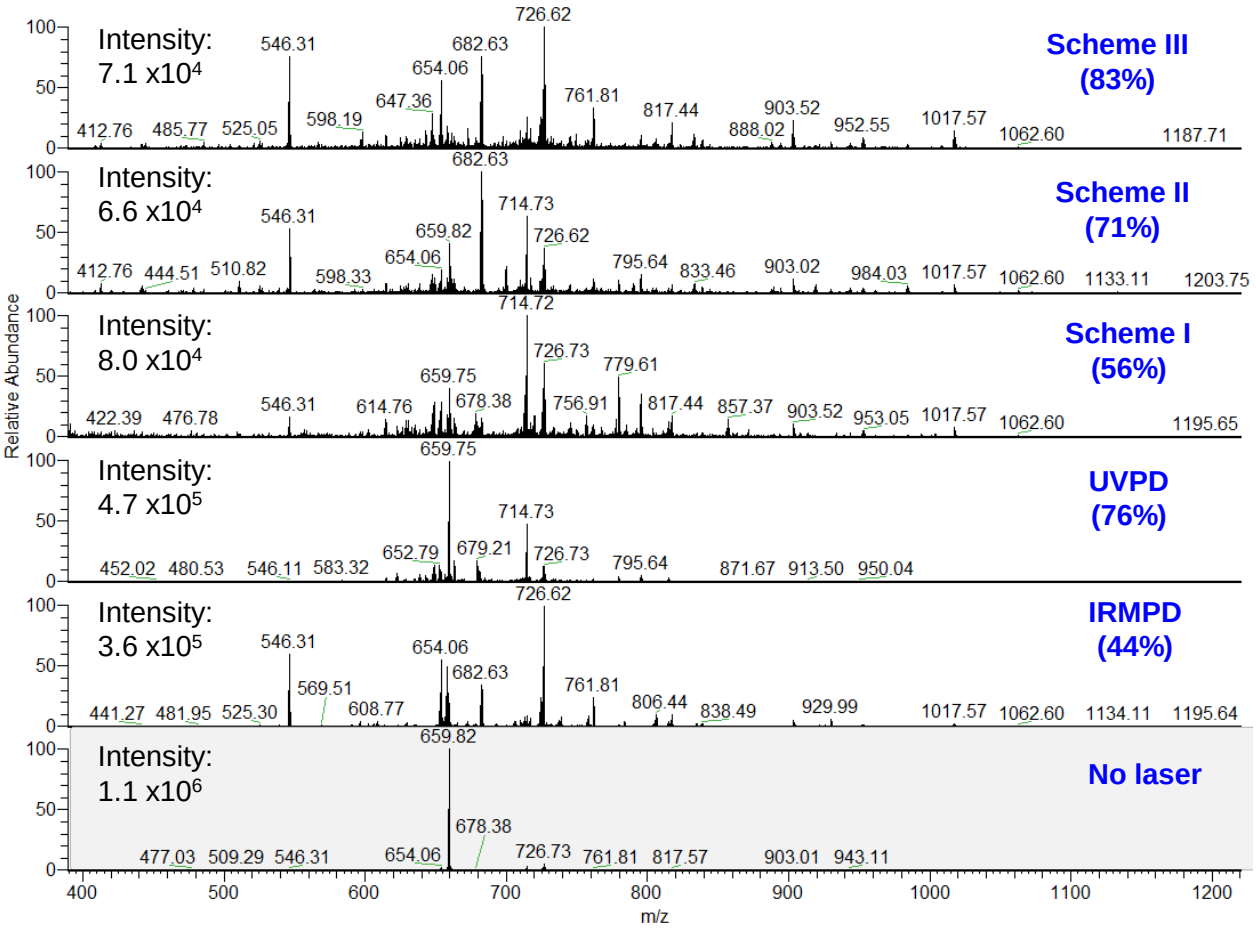

Figure 3. Combined IR and UV (schemes I, II, III), IRMPD and UVPD spectra of the +13 charge state precursor ion (*m/z*=659.8249) of ubiquitin. Isolation spectrum with no activation is also presented. Sequence coverages are indicated in brackets.

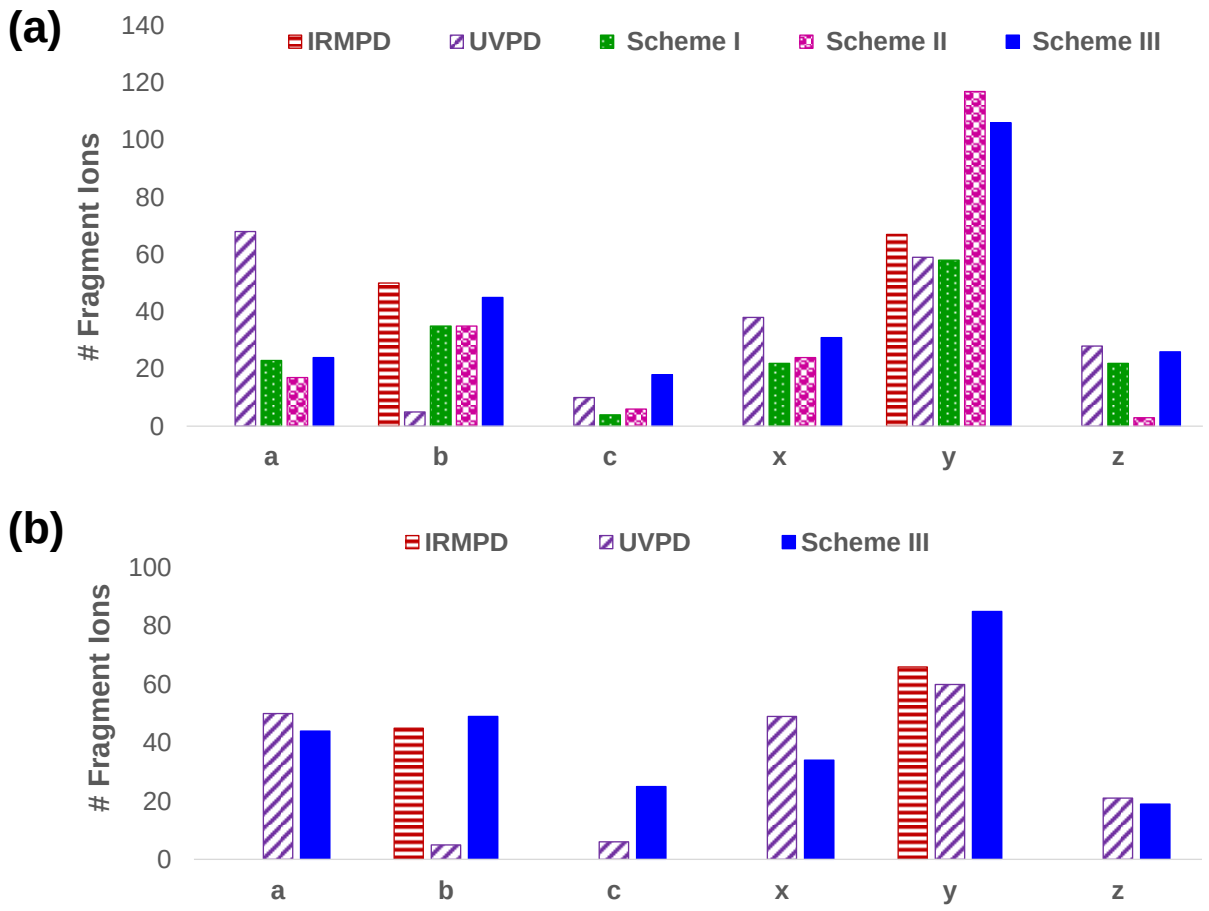

Figure 4. (a) Number of fragment ions detected by IRMPD, UVPD, and combined IR and UV (scheme I, II and III) of the +13 charge state precursor ion (*m/z*=659.8249) of ubiquitin. (b) Number of fragment ions detected by IRMPD, UVPD and HiLoPD (scheme III) of the +8 charge states precursor ion (*m/z*=1071.5864) of ubiquitin.

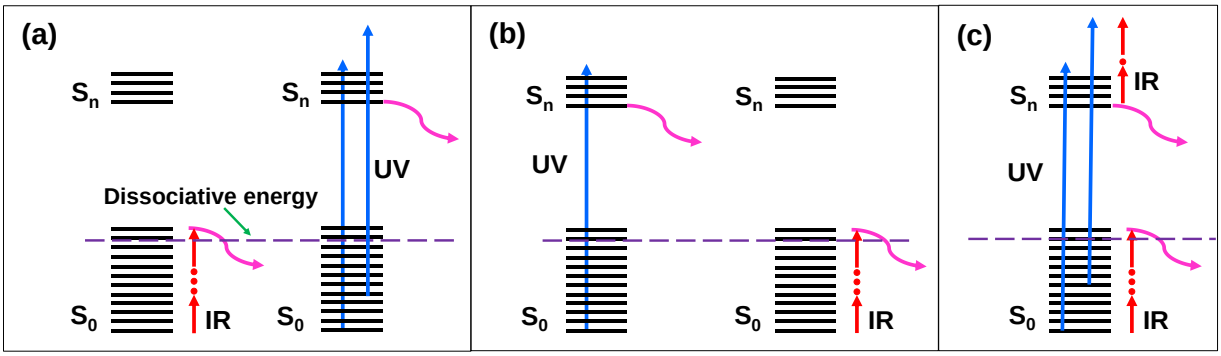

Figure 5. Ground and excited state dissociation channels in scheme I (a), scheme II (b) and scheme III (c)

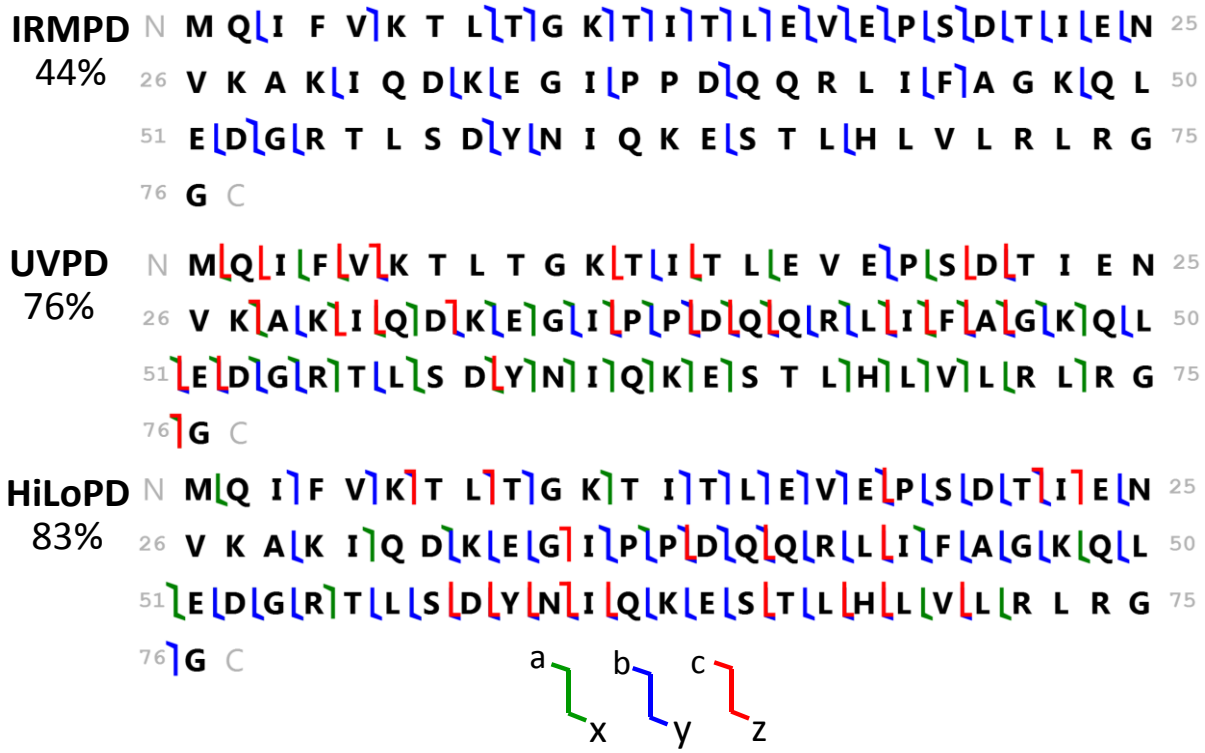

Figure 6. Sequence coverage of the +13 charge state precursor ion (*m/z*=659.8249) of ubiquitin observed by IRMPD, UVPD and HiLoPD (scheme III).

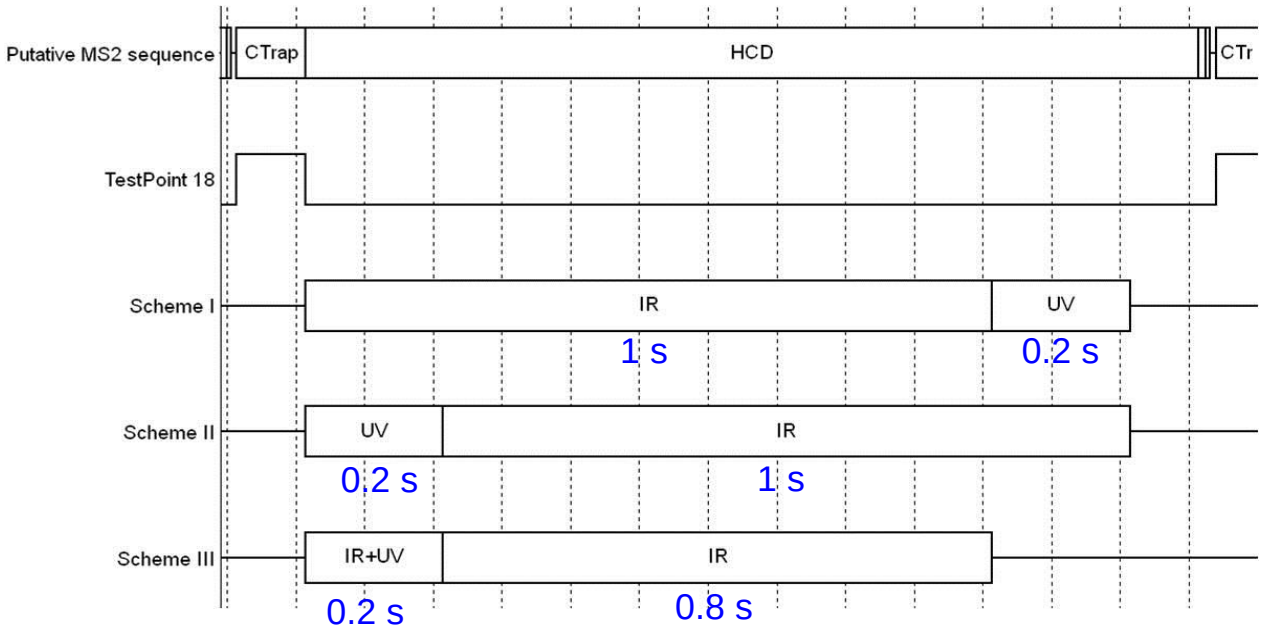

Figure S1. Consecutive and simultaneous irradiations of UV and IR laser in the combined high-low energy photon based method.

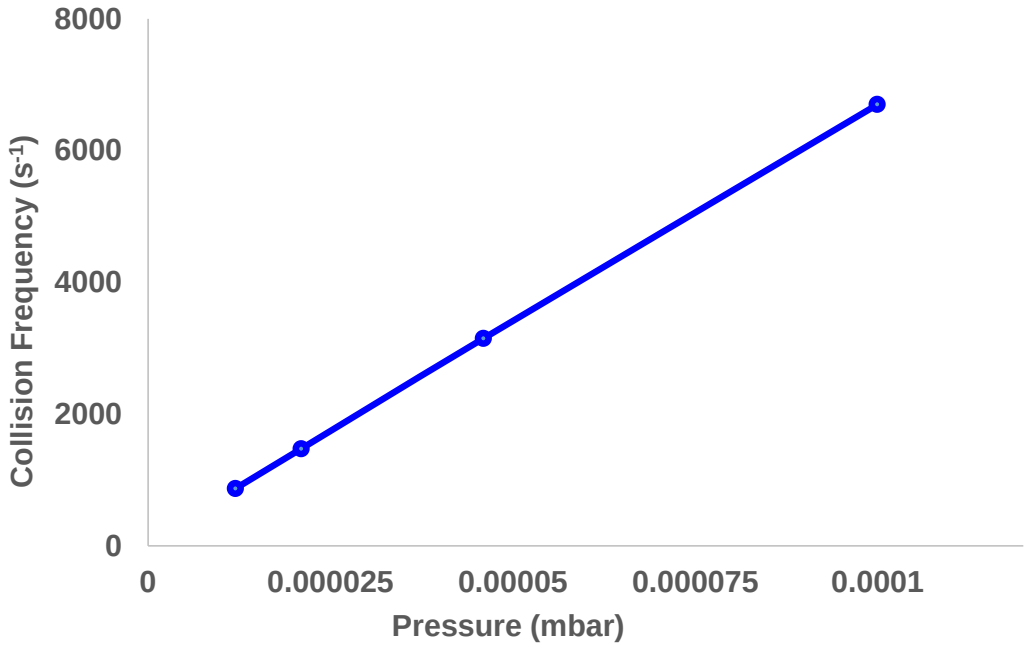

Figure S2. Effect of pressure on the collision frequency (s^{-1}) of the +12 (*m/z*=714.7279) ion of ubiquitin. Collision Cross-Section (CCS) value was taken from the ref. 34.

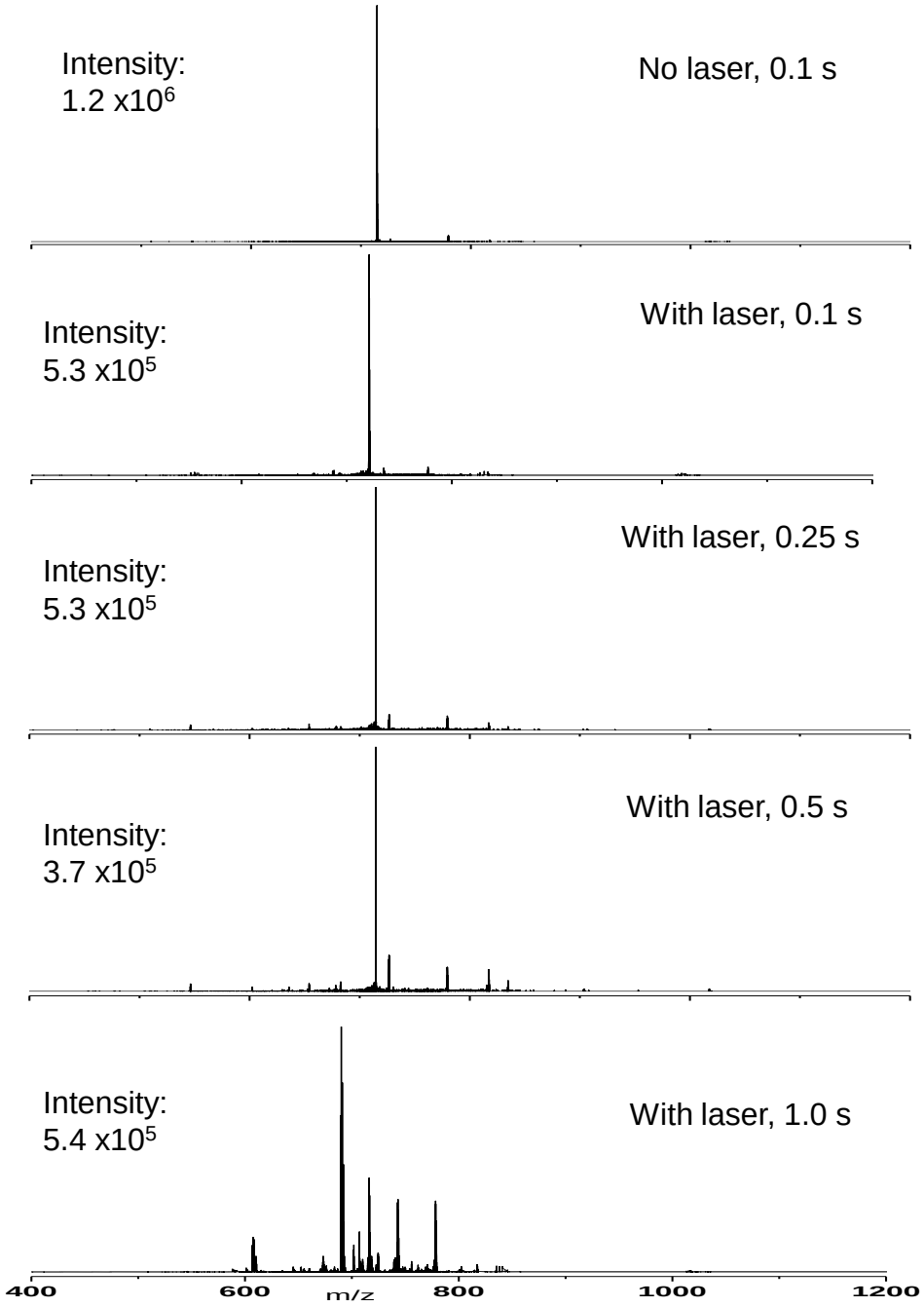

Figure S3. Effect of IRMPD irradiation time (s) on the +12 charge state precursor ion (*m/z*=714.7279) of ubiquitin at low pressure in the HCD cell (9.3 x10^{-6} mbar).

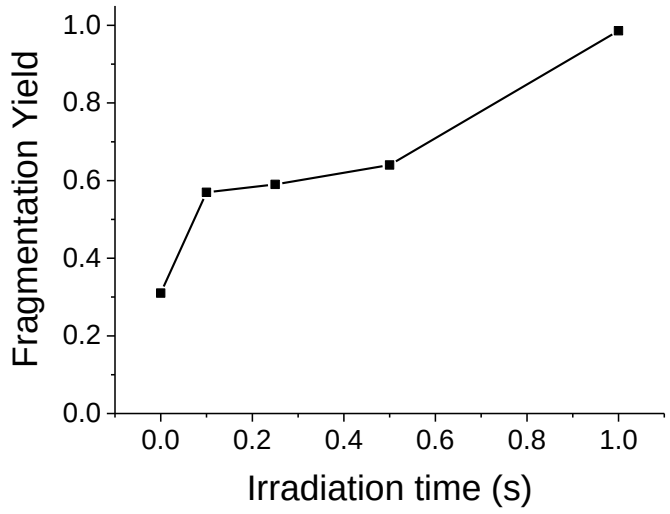

Figure S4. Fragmentation yield based on the IRMPD irradiation time (s) for the +12 charge state precursor ion (*m/z*=714.7279) of ubiquitin at the lowest HCD pressure (~9.3 x10^{-6} mbar). Fragmentation yield = Σ(photofragments)/Σ(photofragments+precursor)

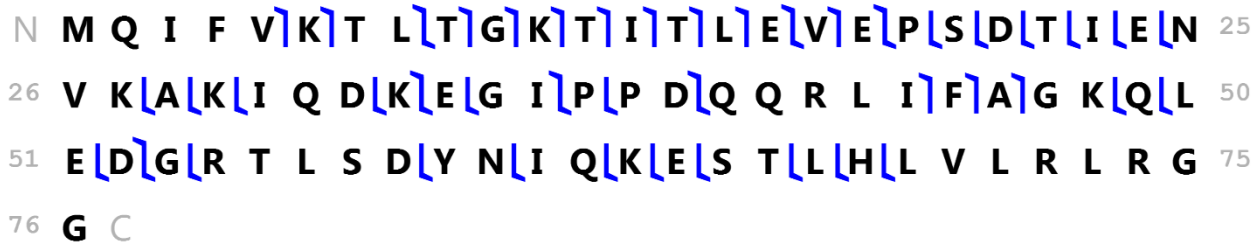

Figure S5. IRMPD sequence coverage (59%) of the +12 charge state precursor ion (*m/z*=714.7279) of ubiquitin.

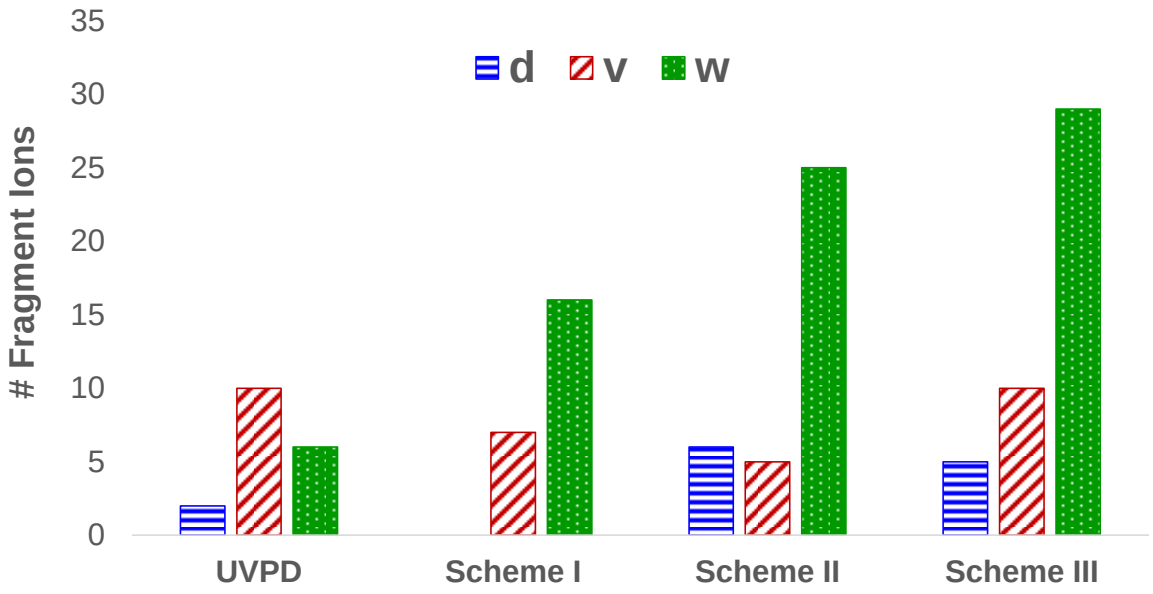

Figure S6. Number of secondary fragment ions (d, v and w) detected by UVPD, and combined IR and UV (scheme I, II and III) of the +13 charge state precursor ion (*m/z*=659.8249) of ubiquitin.

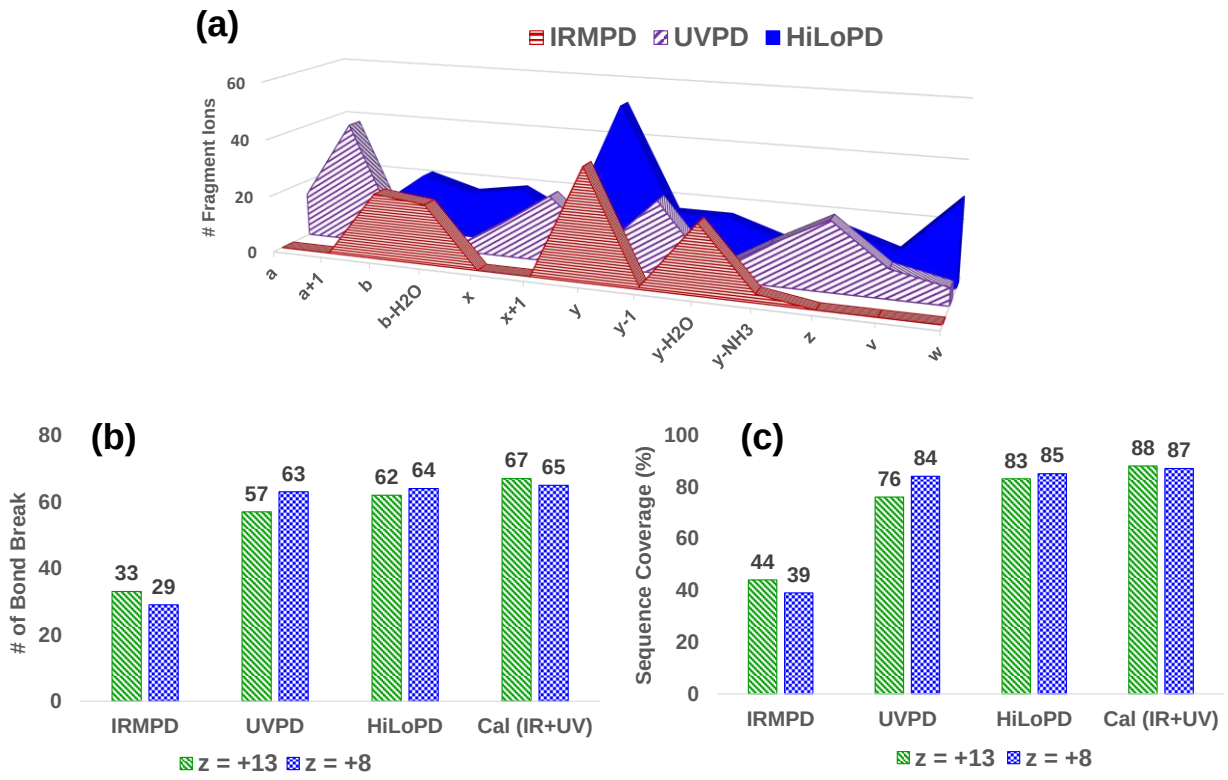

Figure S7. (a) Comparative view of fragment ion types generated by IRMPD, UVPD and HiLoPD (scheme III) of the +13 charge state precursor ion (*m/z*=659.8249) of ubiquitin. (b) Number of bond breaks (c) Sequence coverage (%) obtained by IRMPD, UVPD, HiLoPD (scheme III), and theoretically combined IR and UV (Calculated (IR+UV)) of the +13 (*m/z*=659.8249) and +8 (*m/z*=1071.5864) charge state precursor ions of ubiquitin.

Table S1. Exact masses and assignments of ions detected by IRMPD of the +12 charge state precursor ion (*m/z*=714.7279) of ubiquitin.

Serial	Experimental m/z	Experimental Mass	Theoretical Mass	Assignment	Mass Difference (ppm)
1	619.3269	618.3196	618.3200	$(b_5)^+$	-0.1412
2	442.2950	882.5755	882.5763	$(y_8)^{2+}$	-0.3207
3	472.2755	942.5364	942.5366	$(b_8\text{-}H_2O)^{2+}$	-0.0943
4	961.5536	960.5464	960.5467	$(b_8)^+$	-0.1009
5	510.8247	1019.6348	1019.6352	$(y_9)^{2+}$	-0.1634
6	1062.6016	1061.5943	1061.5943	$(b_9)^+$	-0.0121
7	1119.6230	1118.6158	1118.6158	$(b_{10})^+$	0.0040
8	567.3669	1132.7192	1132.7193	$(y_{10})^{2+}$	-0.0262
9	1247.7173	1246.7100	1246.7108	$(b_{11})^+$	-0.3026
10	624.3626	1246.7107	1246.7108	$(b_{11})^{2+}$	-0.0202
11	652.4030	1302.7915	1302.7890	$(y_{12}\text{-}H_2O)^{2+}$	1.0252
12	441.2731	1320.7976	1320.7990	$(y_{12})^{3+}$	-0.5547
13	674.8868	1347.7591	1347.7584	$(b_{12})^{2+}$	0.2703
14	716.9240	1431.8334	1431.8315	$(y_{13}\text{-}H_2O)^{2+}$	0.7469
15	478.2837	1431.8292	1431.8315	$(y_{13}\text{-}H_2O)^{3+}$	-0.9475
16	722.4239	1442.8332	1442.8325	$(b_{13}\text{-}H_2O)^{2+}$	0.2930
17	481.9510	1442.8313	1442.8325	$(b_{13}\text{-}H_2O)^{3+}$	-0.4735
18	484.2872	1449.8398	1449.8416	$(y_{13})^{3+}$	-0.7121
19	731.4271	1460.8396	1460.8425	$(b_{13})^{2+}$	-1.1659
20	772.9465	1543.8785	1543.8802	$(b_{14}\text{-}H_2O)^{2+}$	-0.6672
21	780.9623	1559.9100	1559.9265	$(y_{14}\text{-}H_2O)^{2+}$	-6.6601
22	781.9514	1561.8882	1561.8902	$(b_{14})^{2+}$	-0.7948
23	526.9856	1577.9351	1577.9365	$(y_{14})^{3+}$	-0.5749
24	553.3282	1656.9626	1656.9642	$(b_{15}\text{-}H_2O)^{3+}$	-0.6510
25	829.4881	1656.9617	1656.9642	$(b_{15}\text{-}H_2O)^{2+}$	-1.0141
26	838.4936	1674.9727	1674.9742	$(b_{15})^{2+}$	-0.6172
27	845.4823	1688.9501	1688.9686	$(y_{15}\text{-}NH_3)^{2+}$	-7.4531
28	563.9960	1688.9663	1688.9686	$(y_{15}\text{-}NH_3)^{3+}$	-0.9175
29	596.3423	1786.0052	1786.0068	$(b_{16}\text{-}H_2O)^{3+}$	-0.6470
30	894.0103	1786.0061	1786.0068	$(b_{16}\text{-}H_2O)^{2+}$	-0.2839
31	602.3461	1804.0166	1804.0168	$(b_{16})^{3+}$	-0.0888
32	903.0156	1804.0167	1804.0168	$(b_{16})^{2+}$	-0.0484
33	607.3666	1819.0781	1819.0792	$(y_{16})^{3+}$	-0.4297

34	472.2755	1885.0727	1885.0752	$(b_{17}\text{-}H_2O)^{4+}$	-1.0141
35	943.5444	1885.0743	1885.0752	$(b_{17}\text{-}H_2O)^{2+}$	-0.3686
36	629.3654	1885.0743	1885.0752	$(b_{17}\text{-}H_2O)^{3+}$	-0.3686
37	952.5470	1903.0795	1903.0852	$(b_{17})^{2+}$	-2.3116
38	476.7772	1903.0799	1903.0852	$(b_{17})^{4+}$	-2.1503
39	635.3695	1903.0867	1903.0852	$(b_{17})^{3+}$	0.5930
40	672.3803	2014.1191	2014.1178	$(b_{18}\text{-}H_2O)^{3+}$	0.5230
41	1008.0658	2014.1171	2014.1178	$(b_{18}\text{-}H_2O)^{2+}$	-0.2839
42	509.0387	2032.1258	2032.1278	$(b_{18})^{4+}$	-0.8149
43	1017.0706	2032.1267	2032.1278	$(b_{18})^{2+}$	-0.4518
44	693.7323	2078.1752	2078.1754	$(y_{18}\text{-}H_2O)^{3+}$	-0.0842
45	694.0634	2079.1682	2079.1594	$(y_{18}\text{-}NH_3)^{3+}$	3.5404
46	520.8014	2079.1765	2079.1594	$(y_{18}\text{-}NH_3)^{4+}$	6.8888
47	525.0534	2096.1843	2096.1854	$(y_{18})^{4+}$	-0.4539
48	1049.1000	2096.1854	2096.1854	$(y_{18})^{2+}$	-0.0101
49	699.7359	2096.1859	2096.1854	$(y_{18})^{3+}$	0.1916
50	575.3171	2297.2394	2297.2366	$(y_{20}\text{-}1)^{4+}$	1.1417
51	668.1270	2668.4788	2668.4772	$(y_{23})^{4+}$	0.6273
52	542.5047	2707.4871	2707.4887	$(y_{24}\text{-}H_2O)^{5+}$	-0.6409
53	909.5066	2725.4981	2725.4987	$(y_{24})^{3+}$	-0.2441
54	546.1070	2725.4988	2725.4987	$(y_{24})^{5+}$	0.0383
55	682.3843	2725.5082	2725.4987	$(y_{24})^{4+}$	3.8306
56	565.5108	2822.5175	2822.5156	$(y_{25}\text{-}H_2O)^{5+}$	0.7549
57	569.1123	2840.5249	2840.5256	$(y_{25})^{5+}$	-0.3006
58	711.1390	2840.5270	2840.5256	$(y_{25})^{4+}$	0.5466
59	771.6700	3082.6509	3082.6523	$(y_{27})^{4+}$	-0.5628
60	639.5475	3192.7011	3192.7009	$(y_{28}\text{-}H_2O)^{5+}$	0.0973
61	533.1234	3192.6967	3192.7009	$(y_{28}\text{-}H_2O)^{6+}$	-1.6777
62	799.4320	3193.6989	3193.6849	$(y_{28}\text{-}NH_3)^{4+}$	5.6584
63	643.1498	3210.7128	3210.7109	$(y_{28})^{5+}$	0.7766
64	694.1793	3465.8612	3465.8566	$(y_{31}\text{-}1)^{5+}$	1.8639
65	723.5956	3612.9375	3612.9250	$(y_{32}\text{-}1)^{5+}$	5.0469
66	925.7614	3699.0166	3699.0168	$(b_{33})^{4+}$	-0.0767
67	1000.5507	3998.1737	3998.1649	$(b_{36})^{4+}$	3.5502
68	847.8688	4234.3078	4234.3092	$(y_{37}\text{-}H_2O)^{5+}$	-0.5602
69	706.7258	4234.3113	4234.3092	$(y_{37}\text{-}H_2O)^{6+}$	0.8518
70	605.9086	4234.3089	4234.3092	$(y_{37}\text{-}H_2O)^{7+}$	-0.1165
71	851.4708	4252.3176	4252.3192	$(y_{37})^{5+}$	-0.6475
72	608.4812	4252.3177	4252.3192	$(y_{37})^{7+}$	-0.6072
73	709.7283	4252.3262	4252.3192	$(y_{37})^{6+}$	2.8220
74	862.4674	4307.3006	4307.2974	$(b_{39})^{5+}$	1.3071

75	745.0730	4464.3945	4464.3989	$(y_{39})^{6+}$	-1.7771
76	913.2980	4561.4537	4561.4517	$(y_{40})^{5+}$	0.8210
77	652.6437	4561.4547	4561.4517	$(y_{40})^{7+}$	1.2244
78	571.1881	4561.4547	4561.4517	$(y_{40})^{8+}$	1.2244
79	789.6001	4731.5568	4731.5572	$(y_{42})^{6+}$	-0.1553
80	808.1062	4842.5936	4842.5898	$(y_{43}\text{-}H_2O)^{6+}$	1.5497
81	969.5244	4842.5856	4842.5898	$(y_{43}\text{-}H_2O)^{5+}$	-1.6777
82	692.8055	4842.5877	4842.5898	$(y_{43}\text{-}H_2O)^{7+}$	-0.8305
83	973.1268	4860.5978	4860.5998	$(y_{43})^{5+}$	-0.7968
84	811.1087	4860.6087	4860.5998	$(y_{43})^{6+}$	3.6006
85	990.1455	4945.6909	4945.6838	$(b_{44})^{5+}$	2.8845
86	832.4553	4988.6881	4988.6947	$(y_{44})^{6+}$	-2.6768
87	995.1429	4970.6780	4970.6847	$(y_{44}\text{-}H_2O)^{5+}$	-2.7105
88	713.6781	4988.6955	4988.6947	$(y_{44})^{7+}$	0.3086
89	998.7464	4988.6958	4988.6947	$(y_{44})^{5+}$	0.4297
90	624.5949	4988.7011	4988.6947	$(y_{44})^{8+}$	2.5678
91	1019.5578	5092.7542	5092.7522	$(b_{45})^{5+}$	0.8230
92	1033.7586	5163.7818	5163.7893	$(b_{46})^{5+}$	-3.0136
93	891.8188	5344.8673	5344.8643	$(y_{47})^{6+}$	1.2042
94	669.1164	5344.8692	5344.8643	$(y_{47})^{8+}$	1.9707
95	782.8556	5472.9547	5472.9593	$(y_{48})^{7+}$	-1.8457
96	694.0061	5543.9936	5543.9964	$(y_{49})8+$	-1.1235
97	793.0071	5543.9990	5543.9964	$(y_{49})^{7+}$	1.0550
98	797.1548	5573.0319	5573.0219	$(b_{50}\text{-}NH_3)^{7+}$	4.0447
99	728.0168	5816.0763	5816.1078	$(b_{52}\text{-}H_2O)^{8+}$	-12.7256
100	834.4510	5834.1059	5834.1179	$(b_{52})^{7+}$	-4.8250
101	973.3599	5834.1156	5834.1179	$(b_{52})^{6+}$	-0.9117
102	734.4072	5867.1996	5867.1927	$(y_{52}\text{-}H_2O)^{8+}$	2.7963
103	841.7505	5885.2023	5885.2027	$(y_{52})^{7+}$	-0.1553
104	736.6576	5885.2029	5885.2027	$(y_{52})^{8+}$	0.0867
105	654.9188	5885.2041	5885.2027	$(y_{52})^{9+}$	0.5709
106	750.5386	5996.2509	5996.2353	$(y_{53}\text{-}H_2O)^{8+}$	6.3102
107	669.2568	6014.2439	6014.2453	$(y_{53})^{9+}$	-0.5547
108	752.7878	6014.2493	6014.2453	$(y_{53})^{8+}$	1.6238
109	860.1852	6014.2497	6014.2453	$(y_{53})^{7+}$	1.7852
110	888.2028	6210.3680	6210.3670	$(y_{55}\text{-}H_2O)^{7+}$	0.4040
111	777.3024	6210.3632	6210.3670	$(y_{55}\text{-}H_2O)^{8+}$	-1.5325
112	890.7747	6228.3719	6228.3770	$(y_{55})^{7+}$	-2.0635
113	779.5545	6228.3775	6228.3770	$(y_{55})^{8+}$	0.1957
114	693.0497	6228.3814	6228.3770	$(y_{55})^{9+}$	1.7690
115	791.6810	6325.3978	6325.3939	$(y_{56}\text{-}H_2O)^{8+}$	1.5578

116	793.9322	6343.3994	6343.4040	$(y_{56})^{8+}$	-1.8376
117	907.2074	6343.4006	6343.4040	$(y_{56})^{7+}$	-1.3535
118	705.8309	6343.4126	6343.4040	$(y_{56})^{9+}$	3.4876
119	642.2506	6412.4331	6412.4260	$(y_{57}\text{-}H_2O)^{10+}$	2.8770
120	715.5004	6430.4379	6430.4360	$(y_{57})^{9+}$	0.7726
121	804.8127	6430.4422	6430.4360	$(y_{57})^{8+}$	2.5073
122	930.9321	6509.4734	6509.4787	$(y_{58}\text{-}H_2O)^{7+}$	-2.1498
123	814.6934	6509.4887	6509.4787	$(y_{58}\text{-}H_2O)^{8+}$	4.0227
124	724.2860	6509.5082	6509.4787	$(y_{58}\text{-}H_2O)^{9+}$	11.8896
125	651.9559	6509.4864	6509.4787	$(y_{58}\text{-}H_2O)^{10+}$	3.0948
126	933.5059	6527.4907	6527.4887	$(y_{58})^{7+}$	0.7887
127	653.7569	6527.4959	6527.4887	$(y_{58})^{10+}$	2.8865
128	816.9452	6527.5037	6527.4887	$(y_{58})^{8+}$	6.0333
129	726.2875	6527.5220	6527.4887	$(y_{58})^{9+}$	13.4160
130	830.8218	6638.5165	6638.5209	$(y_{59}\text{-}H_2O)^{8+}$	-1.7584
131	738.6202	6638.5166	6638.5209	$(y_{59}\text{-}H_2O)^{9+}$	-1.7181
132	664.8598	6638.5248	6638.5209	$(y_{59}\text{-}H_2O)^{10+}$	1.5900
133	674.7674	6737.6043	6737.5897	$(y_{60}\text{-}H_2O)^{10+}$	5.8785
134	845.4571	6755.5813	6755.5997	$(y_{60})^{8+}$	-7.4412
135	751.6300	6755.6046	6755.5997	$(y_{60})^{9+}$	1.9586
136	676.5690	6755.6176	6755.5997	$(y_{60})^{10+}$	7.2032
137	687.6700	6866.6275	6866.6319	$(y_{61}\text{-}H_2O)^{10+}$	-1.7584
138	698.9793	6979.7201	6979.7160	$(y_{62}\text{-}H_2O)^{10+}$	1.6707
139	845.3499	7599.0656	7599.0699	$(y_{68})^{9+}$	-1.7408
140	712.8100	8541.6322	8541.6056	$M\text{-}H_2O)^{12+}$	10.7413
141	777.5168	8541.6059	8541.6056	$(M\text{-}H_2O)^{11+}$	0.1311

Table S2. Exact masses and assignments of ions detected by UVPD of the 13+ charge state precursor ion (*m/z*=659.8249) of ubiquitin.

Serial	Experimental m/z	Experimental Mass	Theoretical Mass	Assignment	Mass Difference (ppm)
1	585.3273	584.3200	584.3269	$(x_5+1)^+$	-11.7315
2	636.3491	635.3418	635.3463	$(c_5)^+$	-7.0041
3	730.3975	729.3902	729.3884	$(b_6-NH_3)^+$	0.7366
4	568.3179	1134.6212	1134.6339	$(c_{10}-1)^{2+}$	-11.2371
5	493.7830	1918.1069	1918.1107	$(z_{17}+1)^{4+}$	-1.5330
6	509.0394	2032.1286	2032.1278	$(b_{18})^{4+}$	0.3838
7	521.0490	2080.1671	2080.1667	$(z_{18})^{4+}$	0.2115
8	531.8007	2123.1737	2123.1725	$(x_{18}+1)^{4+}$	0.5581
9	550.0569	2196.1985	2196.2010	$(z_{19}+1)^{4+}$	1.0086
10	553.3015	2209.1768	2209.1962	$(y_{19}-2)^{4+}$	-8.7928
11	571.3097	2281.2098	2281.2179	$(y_{20}-NH_3)^{4+}$	-3.5393
12	582.3146	2325.2294	2325.2315	$(x_{20}+1)^{4+}$	-0.8967
13	603.5877	2410.3219	2410.3206	$(y_{21}-1)^{4+}$	0.5269
14	610.3356	2437.3132	2437.3077	$(x_{21})^{4+}$	2.2484
15	624.8459	2495.3543	2495.3496	$(y_{22}-NH_3)^{4+}$	1.8939
16	531.2975	2651.4512	2651.4512	$(y_{23}-NH_3)^{5+}$	-0.0166
17	534.5014	2667.4707	2667.4694	$(y_{23}-1)^{5+}$	0.4799
18	539.8996	2694.4614	2694.4565	$(x_{23})^{5+}$	1.8148
19	540.3007	2696.4672	2696.4722	$(x_{23}+2)^{5+}$	2.0010
20	542.7035	2708.4809	2708.4727	$(y_{24}-NH_3)^{5+}$	3.0261
21	545.9058	2724.4926	2724.4909	$(y_{24}-1)^{5+}$	0.6313
22	551.5049	2752.4881	2752.4858	$(x_{24}+1)^{5+}$	0.8374
23	565.9090	2824.5085	2824.5069	$(z_{25})^{5+}$	0.5736
24	568.9111	2839.5193	2839.5178	$(y_{25}-1)^{5+}$	0.5212
25	574.5104	2867.5155	2867.5127	$(x_{25}+1)^{5+}$	0.9642
26	591.7179	2953.5529	2953.5495	$(z_{26})^{5+}$	1.1613
27	594.7201	2968.5640	2968.5604	$(y_{26}-1)^{5+}$	1.2094
28	594.9207	2969.5674	2969.5682	$(y_{26})^{5+}$	-0.2812
29	747.9096	2987.6091	2987.6253	$(a_{27})^{4+}$	-5.4107
30	600.3184	2996.5558	2996.5553	$(x_{26}+1)^{5+}$	0.1585
31	759.1652	3032.6318	3032.6465	$(c_{27})^{4+}$	-4.8407
32	771.6674	3082.6406	3082.6523	$(y_{27})^{4+}$	-3.7938
33	638.5621	3187.7743	3187.7652	$(a_{29}+1)^{5+}$	2.8672
34	554.4684	3320.7665	3320.7958	$(y_{29}-H_2O)^{6+}$	-8.8289
35	557.3090	3337.8103	3337.7980	$(y_{29}-1)^{6+}$	3.6821

36	557.4670	3338.7582	3338.8058	$(y_{29})^{6+}$	-14.2671
37	564.3095	3379.8132	3379.8085	$(z_{30})^{6+}$	1.3817
38	566.8051	3394.7869	3394.8195	$(y_{30}-1)^{6+}$	-9.5940
39	571.4766	3422.8158	3422.8144	$(x_{30}+1)^{6+}$	0.4134
40	686.7889	3428.9079	3428.9078	$(a_{31}+1)^{5+}$	0.0292
41	575.8169	3448.8578	3448.8300	$(z_{31}-2)^{6+}$	8.0636
42	576.1492	3450.8516	3450.8456	$(z_{31})^{6+}$	1.7271
43	578.6503	3465.8583	3465.8566	$(y_{31}-1)^{6+}$	0.4963
44	583.3160	3493.8523	3493.8515	$(x_{31}+1)^{6+}$	0.2304
45	718.5945	3587.9360	3587.9481	$(c_{32})^{5+}$	-3.3808
46	600.6605	3597.9192	3597.9141	$(z_{32})^{6+}$	1.4314
47	607.8281	3640.9251	3640.9199	$(x_{32}+1)^{6+}$	1.4268
48	735.4093	3672.0102	3672.0297	$(a_{33}+1)^{5+}$	-5.3104
49	613.0128	3672.0330	3672.0297	$(a_{33}+1)^{6+}$	0.8987
50	619.5079	3711.0040	3710.9981	$(z_{33})^{6+}$	1.5872
51	622.0095	3726.0133	3726.0090	$(y_{33}-1)^{6+}$	1.1406
52	626.5074	3753.0005	3752.9961	$(x_{33})^{6+}$	1.1617
53	631.5133	3783.0361	3783.0385	$(a_{34}-NH_3)^{6+}$	-0.6249
54	634.5204	3801.0786	3801.0723	$(a_{34}+1)^{6+}$	1.6600
55	638.1894	3823.0927	3823.0749	$(y_{34}-NH_3)^{6+}$	4.6470
56	768.8249	3839.0884	3839.0931	$(y_{34}-1)^{5+}$	-1.2268
57	640.8580	3839.1045	3839.0931	$(y_{34}-1)^{6+}$	2.9669
58	772.6254	3858.0904	3858.0938	$(a_{35}+1)^{5+}$	-0.8683
59	644.0256	3858.1101	3858.0938	$(a_{35}+1)^{6+}$	4.2378
60	791.6423	3953.1750	3953.1440	$(a_{36}-NH_3)^{5+}$	7.8459
61	565.7450	3953.1638	3953.1440	$(a_{36}-NH_3)^{7+}$	5.0127
62	662.8653	3971.1479	3971.1778	$(a_{36}+1)^{6+}$	-7.5318
63	568.3179	3971.1743	3971.1778	$(a_{36}+1)^{7+}$	-0.8839
64	795.2429	3971.1780	3971.1778	$(a_{36}+1)^{5+}$	0.0478
65	796.8315	3979.1210	3979.1760	$(y_{35}-NH_3)^{5+}$	-13.8330
66	571.7492	3995.1934	3995.1942	$(y_{35}-1)^{7+}$	-0.2052
67	800.4369	3997.1479	3997.2099	$(y_{35}+1)^{5+}$	-15.5033
68	671.5456	4023.2328	4023.1891	$(x_{35}+1)^{6+}$	10.8533
69	579.6100	4050.2191	4050.1967	$(a_{37}-NH_3)^{7+}$	5.5197
70	582.1800	4068.2092	4068.2306	$(a_{37}+1)^{7+}$	-5.2529
71	814.6537	4068.2319	4068.2306	$(a_{37}+1)^{5+}$	0.3269
72	679.0460	4068.2324	4068.2306	$(a_{37}+1)^{6+}$	0.4498
73	587.8996	4108.2459	4108.2419	$(z_{36})^{7+}$	0.9834
74	590.0437	4123.2546	4123.2528	$(y_{36}-2)^{7+}$	0.4366
75	594.0438	4151.2554	4151.2477	$(x_{36}+2)^{7+}$	1.8512
76	693.0507	4152.2604	4152.2555	$(x_{36}+2)^{6+}$	1.1704

77	595.8994	4164.2445	4164.2755	$(a_{38})^{7+}$	-7.4455
78	834.0613	4165.2703	4165.2833	$(a_{38}+1)^{5+}$	-3.1282
79	695.2207	4165.2807	4165.2833	$(a_{38}+1)^{6+}$	-0.6314
80	699.5472	4191.2395	4191.2626	$(b_{38}-1)^{6+}$	-5.5103
81	599.8982	4192.2361	4192.2704	$(b_{38})^{7+}$	-8.1865
82	606.1942	4236.3086	4236.3004	$(z_{37})^{7+}$	1.9262
83	608.4799	4252.3087	4252.3192	$(y_{37})^{7+}$	-2.4704
84	612.3380	4279.3152	4279.3063	$(x_{37}+1)^{7+}$	2.0809
85	618.6285	4323.3482	4323.3156	$(c_{39}-1)^{7+}$	7.5289
86	618.9110	4325.3108	4325.3313	$(c_{39}+1)^{7+}$	-4.7395
87	871.2728	4351.3278	4351.3274	$(z_{38})^{5+}$	0.0965
88	726.2288	4351.3290	4351.3274	$(z_{38})^{6+}$	0.3723
89	622.6265	4351.3349	4351.3274	$(z_{38})^{7+}$	1.7282
90	624.7706	4366.3434	4366.3383	$(y_{38}-1)^{7+}$	1.1635
91	628.6260	4393.3314	4393.3254	$(x_{38})^{7+}$	1.3634
92	733.3950	4394.3263	4394.3332	$(x_{38}+1)^{6+}$	-1.5782
93	879.8741	4394.3316	4394.3332	$(x_{38}+1)^{5+}$	-0.3721
94	735.5684	4407.3665	4407.3610	$(a_{40})^{6+}$	1.2422
95	630.6328	4407.3786	4407.3610	$(a_{40})^{7+}$	3.9876
96	632.2061	4418.3920	4418.3295	$(b_{40}-NH_3)^{7+}$	14.1515
97	636.3491	4447.3929	4447.3725	$(y_{39}-NH_3)^{7+}$	4.5928
98	637.2086	4453.4091	4453.3898	$(c_{40}+1)^{7+}$	4.3338
99	638.4930	4462.4004	4462.3833	$(y_{39}-2)^{7+}$	3.8421
100	558.8069	4462.3967	4462.3833	$(y_{39}-2)^{8+}$	0.8292
101	558.9315	4463.3936	4463.3911	$(y_{39}-1)^{8+}$	0.5646
102	749.5713	4491.3844	4491.3860	$(x_{39}+1)^{6+}$	-0.3551
103	642.6362	4491.4027	4491.3860	$(x_{39}+1)^{7+}$	3.7193
104	758.5784	4545.4269	4545.4329	$(z_{40})^{6+}$	-1.3200
105	650.3622	4545.4843	4545.4329	$(z_{40})^{7+}$	11.3081
106	570.9363	4559.4323	4559.4360	$(y_{40}-2)^{8+}$	-0.8148
107	761.0810	4560.4424	4560.4438	$(y_{40}-1)^{6+}$	-0.3158
108	652.5053	4560.4863	4560.4438	$(y_{40}-1)^{7+}$	9.3105
109	765.5789	4587.4295	4587.4309	$(x_{40})^{6+}$	-0.3117
110	668.6520	4673.5129	4673.5279	$(y_{41}-1)^{7+}$	-3.2096
111	782.9268	4691.5173	4691.5207	$(a_{42})^{6+}$	-0.7279
112	671.3671	4692.5185	4692.5285	$(a_{42}+1)^{7+}$	-2.1396
113	676.6558	4729.5396	4729.5410	$(y_{42}-1)^{7+}$	-0.3013
114	687.5232	4805.6111	4805.6126	$(a_{43}+1)^{7+}$	-0.3121
115	692.8078	4842.6034	4842.5898	$(y_{43}-H_2O)^{7+}$	2.8169
116	695.2361	4859.6020	4859.5919	$(y_{43}-1)^{7+}$	2.0681
117	699.2347	4887.5920	4887.5869	$(x_{43}+1)^{7+}$	1.0506

118	613.5845	4900.6177	4900.6628	$(a_{44}\text{-}NH_3)^{8+}$	-9.2098
119	820.7886	4918.6880	4918.6967	$(a_{44}+1)^{6+}$	-1.7606
120	820.7886	4918.6880	4918.6967	$(a_{44}+1)^{6+}$	-1.7606
121	703.6797	4918.7071	4918.6967	$(a_{44}+1)^{7+}$	2.1225
122	622.4649	4971.6613	4971.6687	$(y_{44}\text{-}NH_3)^{8+}$	-1.4953
123	624.4691	4987.6949	4987.6869	$(_{y44}\text{-}1)^{8+}$	1.6020
124	627.9686	5015.6909	5015.6818	$(x_{44}+1)^{8+}$	1.8093
125	724.6871	5065.7591	5065.7651	$(a_{45}+1)^{7+}$	-1.1785
126	845.3011	5065.7632	5065.7651	$(a_{45}+1)^{6+}$	-0.3692
127	734.8352	5136.7989	5136.8022	$(a_{46}+1)^{7+}$	-0.6385
128	866.6444	5193.8238	5193.8236	$(a_{47}+1)^{6+}$	0.0308
129	742.9833	5193.8320	5193.8236	$(a_{47}+1)^{7+}$	1.6096
130	746.1148	5215.7530	5215.7615	$(z_{46})^{7+}$	-1.6278
131	752.1074	5257.7007	5257.7595	$(x_{46})^{7+}$	-11.1873
132	666.2430	5321.8857	5321.9186	$(a_{48}+2)^{8+}$	-6.1820
133	667.1089	5328.8130	5328.8456	$(z_{47})^{8+}$	-6.1083
134	609.0017	5471.9500	5471.9514	$(y_{48}\text{-}1)^{9+}$	-0.2650
135	696.3897	5563.0596	5563.0612	$(a_{50}+1)^{8+}$	-0.2948
136	620.0076	5570.9963	5570.9835	$(x_{49}+1)^{9+}$	2.3021
137	629.3496	5655.0809	5655.0649	$(y_{50}\text{-}NH_3)^{9+}$	2.8339
138	712.3961	5691.1104	5691.0960	$(a_{51})^{8+}$	2.5294
139	726.8979	5807.1230	5807.1308	$(a_{52}+1)^{8+}$	-1.3380
140	830.5964	5807.1311	5807.1308	$(a_{52}+1)^{7+}$	0.0568
141	733.9007	5863.1428	5863.1444	$(a_{53})^{8+}$	-0.2737
142	734.3986	5867.1308	5867.1923	$(y_{52}\text{-}H_2O)^{8+}$	-10.4750
143	753.4126	6019.2426	6019.2455	$(a_{54})^{8+}$	-0.4843
144	669.9224	6020.2361	6020.2533	$(a_{54}+1)^{9+}$	-2.8637
145	763.9152	6103.2635	6103.2668	$(a_{55}\text{-}NH_3)^{8+}$	-0.5364
146	691.1566	6211.3438	6211.3504	$(z_{55}\text{-}1)^{9+}$	-1.0666
147	622.2438	6212.3657	6212.3583	$(z_{55})^{10+}$	1.1992
148	623.8417	6228.3444	6228.3770	$(y_{55})^{10+}$	-5.2365
149	693.1599	6229.3736	6229.3848	$(y_{55}+1)^{9+}$	-1.8044
150	693.7168	6234.3857	6234.3851	$(a_{56}+1)^{9+}$	0.0994
151	626.5463	6255.3904	6255.3641	$(x_{55}+1)^{10+}$	4.2036
152	633.7473	6327.4001	6327.3852	$(z_{56})^{10+}$	2.3564
153	716.1649	6436.4183	6436.4441	$(a_{58}+1)^{9+}$	-4.0007
154	805.5633	6436.4481	6436.4441	$(a_{58}+1)^{8+}$	0.6292
155	718.3884	6456.4297	6456.4153	$(x_{57})^{9+}$	2.2381
156	594.2325	6525.4770	6525.4731	$(y_{58}\text{-}2)^{11+}$	0.5984
157	816.8168	6526.4760	6526.4809	$(y_{58}\text{-}1)^{8+}$	-0.7538
158	726.1717	6526.4795	6526.4809	$(y_{58}\text{-}1)^{9+}$	-0.2176

159	653.6608	6526.5347	6526.4809	$(y_{58}-1)^{10+}$	8.2403
160	734.1736	6598.4965	6598.4996	$(a_{59})^{9+}$	-0.4630
161	825.9476	6599.5224	6599.5074	$(a_{59}+1)^{8+}$	2.2759
162	664.9534	6639.4611	6639.5049	$(y_{59}-NH_3)^{10+}$	-6.5930
163	746.9571	6713.5481	6713.5503	$(a_{60}+1)^{9+}$	-0.3292
164	674.8693	6738.6197	6738.5733	$(y_{60}-NH_3)^{10+}$	6.8896
165	759.4141	6825.6614	6825.6265	$(a_{61})^{9+}$	5.1065
166	692.0735	6910.6622	6910.6216	$(x_{61})^{10+}$	5.8750
167	768.9650	6911.6196	6911.6294	$(x_{61}+1)^{9+}$	-1.4215
168	773.6386	6953.6951	6953.6851	$(a_{62})^{9+}$	1.4345
169	787.9817	7082.7695	7082.7879	$(a_{63}+1)^{9+}$	-2.5993
170	709.3884	7083.8108	7083.7957	$(a_{63}+2)^{10+}$	2.1267
171	792.7589	7125.7573	7125.7612	$(x_{63}+1)^{9+}$	-0.5424
172	720.4863	7194.7906	7194.8321	$(y_{64}-NH_3)^{10+}$	-5.7728
173	722.0888	7210.8151	7210.8227	$(a_{64})^{10+}$	-1.0505
174	722.0888	7210.8151	7210.8503	$(y_{64}-1)^{10+}$	-4.8829
175	811.7703	7296.8652	7296.8871	$(z_{65})^{9+}$	-2.9944
176	730.6955	7296.8818	7296.8871	$(z_{65})^{10+}$	-0.7195
177	739.1967	7381.8946	7381.8760	$(a_{66}-NH_3)^{10+}$	2.5232
178	752.2062	7511.9914	7511.9864	$(a_{67})^{10+}$	0.6596
179	835.7844	7512.9924	7512.9943	$(a_{67}+1)^{9+}$	0.2489
180	752.2064	7512.9924	7512.9943	$(a_{67}+1)^{10+}$	-0.2489
181	690.2807	7582.0080	7582.0435	$(y_{68}-NH_3)^{11+}$	-4.6787
182	766.0105	7650.0323	7650.0532	$(a_{68}+1)^{10+}$	-2.7294
183	696.4663	7650.0491	7650.0532	$(a_{68}+1)^{11+}$	-0.5333
184	700.5686	7695.1740	7695.1276	$(y_{69}-NH_3)^{11+}$	6.0332
185	777.3192	7763.1197	7763.1372	$(a_{69}+1)^{10+}$	-2.2594
186	706.8406	7764.1663	7764.1451	$(a_{69}+2)^{11+}$	2.7350
187	780.6230	7796.1574	7796.1753	$(y_{70}-NH_3)^{10+}$	-2.2927
188	787.1270	7861.2043	7861.1978	$(a_{70})^{10+}$	0.8237
189	721.4824	7925.2266	7925.2779	$(z_{71})^{11+}$	-6.4667
190	722.9445	7941.3094	7941.2966	$(y_{71})^{11+}$	1.6099
191	730.4907	8024.3181	8024.3463	$(z_{72})^{11+}$	-3.5093
192	673.2019	8066.3355	8066.3443	$(x_{72})^{12+}$	-1.0897
193	734.3206	8066.4464	8066.3443	$(x_{72})^{11+}$	12.6588
194	685.5384	8214.3730	8214.4205	$(x_{73}+1)^{12+}$	-5.7856
195	747.7728	8214.4299	8214.4205	$(x_{73}+1)^{11+}$	1.1413
196	747.7727	8214.4299	8214.4205	$(x_{73}+1)^{11+}$	1.1413
197	750.5136	8244.5693	8244.4749	$(a_{73}+1)^{11+}$	11.4525
198	691.3785	8284.4543	8284.4987	$(z_{74})^{12+}$	-5.3630
199	692.5549	8298.5712	8298.5014	$(y_{74}-2)^{12+}$	8.4081

200	699.5558	8382.5818	8382.5418	$(a_{74}\text{-}NH_3)^{12+}$	4.7749
201	702.0551	8412.5738	8412.5573	$(z_{75})^{12+}$	1.9602
202	703.2258	8426.6228	8426.5600	$(y_{75}\text{-}2)^{12+}$	7.4497
203	705.5567	8454.5929	8454.5553	$(x_{75})^{12+}$	4.4426
204	769.7864	8456.5706	8456.5896	$(a_{75})^{11+}$	-2.2497
205	651.5958	8457.6475	8457.5975	$(a_{75}+1)^{13+}$	5.9178
206	709.3884	8500.5730	8500.6030	$(c_{75}\text{-}1)^{12+}$	-3.5309
207	654.9071	8500.6976	8500.6030	$(c_{75}\text{-}1)^{13+}$	11.1269
208	773.8821	8501.6226	8501.6108	$(c_{75})^{11+}$	1.3833
209	712.8979	8542.6875	8542.5896	$(M\text{-}NH_3)^{12+}$	11.4632

Table S3. Exact masses and assignments of ions detected by IRMPD of the +13 charge state precursor ion (*m/z*=659.8249) of Ubiquitin.

Serial	Experimental m/z	Experimental Mass	Theoretical Mass	Assignment	Mass Difference (ppm)
1	619.3274	618.3201	618.3200	$(b_5)^+$	0.0002
2	415.7326	829.4507	829.4521	$(b_7\text{-}H_2O)^{2+}$	-1.6879
3	943.5440	942.5367	942.5366	$(b_8\text{-}H_2O)^+$	0.1061
4	472.2753	942.5361	942.5366	$(b_8\text{-}H_2O)^{2+}$	-0.5305
5	961.5532	960.5459	960.5467	$(b_8)^+$	-0.0008
6	340.8848	1019.6327	1019.6352	$(y_9)^{3+}$	-0.0025
7	510.8243	1019.6341	1019.6352	$(y_9)^{2+}$	-0.0011
8	531.8039	1061.5932	1061.5943	$(b_9)^{2+}$	-0.0011
9	410.5730	1228.6972	1228.7007	$(b_{11}\text{-}H_2O)^{3+}$	-2.8485
10	624.3631	1246.7116	1246.7108	$(b_{11})^{2+}$	0.0009
11	435.2698	1302.7876	1302.7890	$(y_{12}\text{-}H_2O)_{3+}$	0.6417
12	441.2731	1320.7975	1320.7990	$(y_{12})^{3+}$	-0.0015
13	674.8853	1347.7560	1347.7584	$(b_{12})^{2+}$	-0.0024
14	481.9509	1442.8308	1442.8325	$(b_{13}\text{-}H_2O)^{3+}$	-1.1782
15	487.2821	1458.8245	1458.8268	$(b_{13}\text{-}2)^{3+}$	-1.5766
16	731.4255	1460.8365	1460.8425	$(b_{13})^{2+}$	-0.0060
17	487.9538	1460.8396	1460.8425	$(b_{13})^{3+}$	-0.0029
18	772.9462	1543.8778	1543.8802	$(b_{14}\text{-}H_2O)^{2+}$	-1.5545
19	515.6334	1543.8782	1543.8802	$(b_{14}\text{-}H_2O)^{3+}$	-1.2954
20	521.2980	1560.8721	1560.8823	$(b_{14}\text{-}1)^{3+}$	-6.5348
21	781.9512	1561.8878	1561.8902	$(b_{14})^{2+}$	-0.0024
22	553.3281	1656.9625	1656.9642	$(b_{15}\text{-}H_2O)^{3+}$	-1.0260
23	559.3306	1674.9699	1674.9742	$(b_{15})^{3+}$	-0.0043
24	838.4937	1674.9729	1674.9742	$(b_{15})^{2+}$	-0.0013
25	894.0101	1786.0056	1786.0068	$(b_{16}\text{-}H_2O)^{2+}$	-0.6719
26	596.3424	1786.0054	1786.0068	$(b_{16}\text{-}H_2O)^{3+}$	-0.7839
27	903.0153	1804.0161	1804.0168	$(b_{16})^{2+}$	-0.0007
28	602.3460	1804.0163	1804.0168	$(b_{16})^{3+}$	-0.0005
29	629.3656	1885.0750	1885.0752	$(b_{17}\text{-}H_2O)^{3+}$	-0.1061
30	472.2753	1885.0722	1885.0752	$(b_{17}\text{-}H_2O)^{4+}$	-1.5914
31	476.7778	1903.0823	1903.0852	$(b_{17})^{4+}$	-0.0029
32	952.5491	1903.0836	1903.0852	$(b_{17})^{2+}$	-0.0016
33	635.3695	1903.0866	1903.0852	$(b_{17})^{3+}$	0.0014
34	484.2871	1933.1195	1933.1221	$(y_{17})^{4+}$	-0.0026
35	1008.0655	2014.1164	2014.1178	$(b_{18}\text{-}H_2O)_{2+}$	-0.6951
36	672.3783	2014.1132	2014.1178	$(b_{18}\text{-}H_2O)^{3+}$	-2.2839
37	504.5357	2014.1138	2014.1178	$(b_{18}\text{-}H_2O)^{4+}$	-1.9860

38	678.3822	2032.1247	2032.1278	$(b_{18})^{3+}$	-0.0031
39	509.0387	2032.1257	2032.1278	$(b_{18})^{4+}$	-0.0021
40	1017.0705	2032.1264	2032.1278	$(b_{18})2+$	-0.0014
41	525.0535	2096.1847	2096.1854	$(y_{18})^{4+}$	-0.0007
42	699.7363	2096.1870	2096.1854	$(y_{18})^{3+}$	0.0016
43	550.5566	2198.1971	2198.2026	$(b_{20}\text{-}H_2O)^{4+}$	-2.5020
44	555.0599	2216.2104	2216.2126	$(b_{20})^{4+}$	-0.0022
45	832.4524	2494.3355	2494.3656	$(y_{22}\text{-}H_2O)^{3+}$	-12.0672
46	534.7019	2668.4731	2668.4772	$(y_{23})^{5+}$	-0.0041
47	542.5051	2707.4889	2707.4887	$(y_{24}\text{-}H_2O)^{3+}$	0.0739
48	909.5046	2725.4920	2725.4987	$(y_{24})^{3+}$	-0.0067
49	682.3818	2725.4980	2725.4987	$(y_{24})^{4+}$	-0.0007
50	546.1073	2725.5001	2725.4987	$(y_{24})^{5+}$	0.0014
51	569.1122	2840.5245	2840.5256	$(y_{25})^{5+}$	-0.0011
52	639.5476	3192.7016	3192.7009	$(y_{28}\text{-}H_2O)^{5+}$	0.2193
53	533.1232	3192.6957	3192.7009	$(y_{28}\text{-}H_2O)^{6+}$	-1.6287
54	536.1255	3210.7092	3210.7109	$(y_{28})^{6+}$	-0.0017
55	643.1511	3210.7193	3210.7109	$(y_{28})^{5+}$	0.0084
55	593.1574	3552.9009	3552.9114	$(b_{32}\text{-}H_2O)^{6+}$	-2.9553
57	603.3294	3613.9328	3613.9328	$(y_{32})^{6+}$	0.0000
58	614.5078	3681.0032	3681.0063	$(b_{33}\text{-}H_2O)^{6+}$	-0.8422
59	605.9086	4234.3095	4234.3092	$(y_{37}\text{-}H_2O)^{7+}$	0.0708
60	706.8913	4235.3043	4235.2932	$(y_{37}\text{-}NH_3)^{6+}$	2.6208
61	851.4706	4252.3167	4252.3192	$(y_{37})^{5+}$	-0.0025
62	608.4816	4252.3204	4252.3192	$(y_{37})^{7+}$	0.0012
63	709.7296	4252.3340	4252.3192	$(y_{37})^{6+}$	0.0148
64	862.4662	4307.2947	4307.2974	$(b_{39})^{5+}$	-0.0027
65	571.1881	4561.4464	4561.4517	$(y_{40})^{8+}$	-0.0053
66	652.7925	4562.4963	4562.4595	$(y_{40}+1)^{7+}$	8.0658
67	692.8042	4842.5784	4842.5898	$(y_{43}\text{-}H_2O)^{7+}$	-2.3541
68	811.1034	4860.5768	4860.5998	$(y_{43})^{6+}$	-0.0230
69	704.9617	4927.6809	4927.6733	$(b_{44}\text{-}H_2O)^{7+}$	1.5423
70	624.5940	4988.6939	4988.6947	$(y_{44})^{8+}$	-0.0008
71	849.7984	5092.7384	5092.7522	$(b_{45})^{6+}$	-0.0138
72	594.8814	5344.8578	5344.8643	$(y_{47})^{9+}$	-0.0065
73	797.1543	5573.0289	5573.0219	$(b_{50}\text{-}NH_3)^{7+}$	1.2561
74	727.8884	5815.0486	5815.1000	$(b_{52}\text{-}1\text{-}H_2O)^{8+}$	-8.8391
75	831.8774	5816.0908	5816.1078	$(b_{52}\text{-}H_2O)^{7+}$	-2.9229
76	730.1431	5833.0862	5833.1100	$(b_{52}\text{-}1)^{8+}$	-4.0802
77	834.4512	5834.1073	5834.1179	$(b_{52})^{7+}$	-0.0106
78	654.9139	5885.1596	5885.2027	$(y_{52})^{9+}$	-0.0431
79	667.2533	5996.2103	5996.2353	$(y_{53}\text{-}H_2O)^{9+}$	-4.1693
80	752.7841	6014.2144	6014.2453	$(y_{53})^{8+}$	-0.0309

81	669.2551	6014.2305	6014.2453	$(y_{53})^{9+}$	-0.0148
82	679.8181	6109.2971	6109.3193	$(y_{54}\text{-}H_2O)^{9+}$	-3.6338
83	766.9226	6127.3221	6127.3293	$(y_{54})^{8+}$	-0.0072
84	691.1673	6211.4402	6211.3510	$(y_{55}\text{-}NH_3)^{9+}$	14.3608
85	693.0501	6228.3856	6228.3770	$(y_{55})^{9+}$	0.0086
86	703.8285	6325.3906	6325.3939	$(y_{56}\text{-}H_2O)^{9+}$	-6.7314
87	793.9274	6343.3613	6343.4040	$(y_{56})^{8+}$	-0.0427
88	635.3490	6343.4132	6343.4040	$(y_{56})^{10+}$	0.0092
89	705.8314	6343.4171	6343.4040	$(y_{56})^{9+}$	0.0131
90	715.4990	6430.4251	6430.4360	$(y_{57})^{9+}$	-0.0109
91	804.8122	6430.4335	6430.4360	$(y_{57})^{8+}$	-0.0025
92	719.1677	6463.4441	6463.4311	$(b_{58})^{9+}$	0.0130
93	930.9317	6509.4693	6509.4787	$(y_{58}\text{-}H_2O)^{7+}$	-1.4440
94	814.6920	6509.4776	6509.4787	$(y_{58}\text{-}H_2O)^{8+}$	-0.1690
95	724.2892	6509.5369	6509.4787	$(y_{58}\text{-}H_2O)^{9+}$	8.9408
96	651.9622	6509.5496	6509.4787	$(y_{58}\text{-}H_2O)^{10+}$	10.8918
97	816.9435	6527.4895	6527.4887	$(y_{58})^{8+}$	0.0008
98	594.4158	6527.4932	6527.4887	$(y_{58})^{11+}$	0.0045
99	933.5091	6527.5127	6527.4887	$(y_{58})^{7+}$	0.0240
100	830.8221	6638.5189	6638.5213	$(y_{59}\text{-}H_2O)^{8+}$	-0.3615
101	738.6190	6638.5052	6638.5213	$(y_{59}\text{-}H_2O)^{9+}$	-2.4252
102	664.8559	6638.4862	6638.5213	$(y_{59}\text{-}H_2O)^{10+}$	-5.2873
103	666.5582	6655.5089	6655.5235	$(y_{59}\text{-}1)^{10+}$	-2.1937
104	740.6199	6656.5137	6656.5313	$(y_{59})^{9+}$	-0.0176
105	676.5669	6755.5958	6755.5997	$(y_{60})^{10+}$	-0.0039
106	763.9652	6866.6209	6866.6319	$(y_{61}\text{-}H_2O)^{9+}$	-1.6019
107	687.7706	6867.6329	6867.6159	$(y_{61}\text{-}NH_3)^{10+}$	2.4754
108	698.9792	6979.7344	6979.7160	$(y_{62}\text{-}H_2O)^{10+}$	-0.1776
109	751.6293	6755.5985	6755.5997	$(y_{60})^{9+}$	-0.0012
110	787.7582	7080.7621	7080.7637	$(y_{63}\text{-}H_2O)^{9+}$	-0.2260
111	709.0845	7080.7726	7080.7637	$(y_{63}\text{-}H_2O)^{10+}$	1.2569
112	690.1940	7581.0539	7581.0599	$(y_{68}\text{-}H_2O)^{11+}$	-0.7914
113	691.8304	7599.0547	7599.0699	$(y_{68})^{11+}$	-0.0152
114	691.2163	8282.5071	8282.5075	$(y_{74}\text{-}H_2O)^{12+}$	-0.0483
115	755.6021	8300.5426	8300.5175	$(y_{74})^{11+}$	0.0251
116	701.8797	8410.4692	8410.5367	$(b_{74}\text{-}NH_3)^{12+}$	-8.0256
117	777.5160	8541.5963	8541.6062	$(M\text{-}H_2O)^{11+}$	-1.1590
118	712.8113	8541.6481	8541.6062	$(M\text{-}H_2O)^{12+}$	4.9054
119	856.9684	8559.6109	8559.6162	$(M)^{10+}$	-0.6192
120	779.1539	8559.6131	8559.6162	$(M)^{11+}$	-0.3622
121	714.3111	8559.6454	-8561.6318	$(M)^{12+}$	3.4114

Table S4. Exact masses and assignments of ions detected by HiLoPD (scheme III) of the +13 charge state precursor ion (*m/z*=659.8249) of Ubiquitin.

Serial	Experimental m/z	Observed Mass	Theoretical Mass	Assignment	Mass Difference (ppm)
1	373.1900	372.1827	372.1831	$(b_3)^+$	-1.1553
2	556.3269	555.3196	555.3236	$(y_5\text{-}1)^+$	-7.2030
3	292.6662	583.3179	583.3190	$(x_5)^{2+}$	-1.9372
4	617.3121	616.3048	616.3043	$(b_5\text{-}2)^+$	0.8113
5	619.3278	618.3205	618.3200	$(b_5)^+$	0.8895
6	328.2094	654.4042	654.4051	$(z_6)^{2+}$	-1.3142
7	336.2185	670.4225	670.4238	$(y_6)^{2+}$	-1.9764
8	730.3982	729.3910	729.3889	$(b_6\text{-}NH_3)^+$	2.8791
9	747.4210	746.4137	746.4149	$(b_6)^+$	-1.6211
10	382.7276	763.4406	763.4412	$(c_6)^{2+}$	-0.7990
11	384.7450	767.4753	767.4760	$(y_7\text{-}2)^{2+}$	-0.9121

12	796.9503	795.4708	795.4715	$(x_7)^+$	-0.8800
13	398.7427	795.4708	795.4715	$(x_7)^{2+}$	-0.8800
14	434.2858	866.5570	866.5575	$(z_8)^{2+}$	-0.6116
15	442.2949	882.5751	882.5763	$(y_8)^{2+}$	-1.3540
16	943.5451	942.5379	942.5366	$(b_8\text{-}H_2O)^+$	1.3793
17	340.8853	960.5457	960.5467	$(b_8)^{3+}$	-0.9890
18	488.7859	975.5572	975.5573	$(c_8\text{-}2)^{2+}$	-0.1025
19	489.7937	977.5728	977.5730	$(c_8)^{2+}$	-0.1534
20	502.3115	1002.6084	1002.6086	$(z_9\text{-}1)^{2+}$	-0.1995
21	502.8147	1003.6149	1003.6164	$(z_9)^{2+}$	-1.5345
22	340.8853	1019.6341	1019.6352	$(y_9)^{3+}$	-1.0837
23	510.8250	1019.6354	1019.6352	$(y_9)^{2+}$	0.1912
24	522.7989	1043.5832	1043.5843	$(b_9\text{-}H_2O)^{2+}$	-1.0541
25	523.8144	1045.6142	1045.6145	$(x_9)^{2+}$	-0.2582
26	1062.6023	1061.5950	1061.5943	$(b_9)^+$	0.6311
27	567.3667	1132.7189	1132.7193	$(y_{10})^{2+}$	-0.3222
28	406.2543	1215.7410	1215.7325	$(z_{11}\text{-}2)^{3+}$	6.9917
29	406.9223	1217.7451	1217.7482	$(z_{11})^{3+}$	-2.5293
30	610.8695	1219.7244	1219.7237	$(a_{11}\text{+}1)^{2+}$	0.6067
31	412.2623	1233.7652	1233.7669	$(y_{11})^{3+}$	-1.4144
32	421.2584	1260.7533	1260.7540	$(x_{11}\text{+}1)^{3+}$	-0.5830
33	422.5866	1264.7380	1264.7446	$(c_{11}\text{+}1)^{3+}$	-5.2184
34	435.5977	1303.7713	1303.7730	$(y_{12}\text{-}NH_3)^{3+}$	-1.3039
35	441.2736	1320.7990	1320.7990	$(y_{12})^{3+}$	0.0189
36	661.4069	1320.7993	1320.7990	$(y_{12})^{2+}$	0.2461
37	450.2678	1347.7817	1347.7861	$(x_{12}\text{+}1)^{3+}$	-3.2387
38	481.9510	1442.8311	1442.8325	$(b_{13}\text{-}H_2O)^{3+}$	-0.9703
39	484.2873	1449.8402	1449.8416	$(y_{13})^{3+}$	-0.9415
40	725.9286	1449.8427	1449.8416	$(y_{13})^{2+}$	0.7828
41	726.9316	1451.8487	1451.8572	$(y_{13}\text{+}2)^{2+}$	-5.8546
42	731.4283	1460.8420	1460.8425	$(b_{13})^{2+}$	-0.3354
43	772.9470	1543.8794	1543.8802	$(b_{14}\text{-}H_2O)^{2+}$	-0.5182
44	390.9815	1559.8969	1559.8745	$(b_{14}\text{-}2)^{4+}$	14.3601
45	781.9516	1561.8886	1561.8902	$(b_{14})^{2+}$	-1.0052
46	395.4910	1577.9350	1577.9365	$(y_{14})^{4+}$	-0.9665
47	526.9861	1577.9365	1577.9365	$(y_{14})^{3+}$	-0.0158
48	789.9758	1577.9371	1577.9365	$(y_{14})^{2+}$	0.3644
49	829.4889	1656.9632	1656.9642	$(b_{15}\text{-}H_2O)^{2+}$	-0.6035
50	553.3281	1656.9625	1656.9642	$(b_{15}\text{-}H_2O)^{3+}$	-1.0260
51	838.4945	1674.9745	1674.9742	$(b_{15})^{2+}$	0.1612
52	423.2495	1688.9689	1688.9685	$(z_{15}\text{-}1)^{4+}$	0.2368

53	845.9903	1689.9661	1689.9763	$(z_{15})_{2+}$	-6.0593
54	563.9961	1689.9661	1689.9763	$(z_{15})^{3+}$	-6.0593
55	427.2536	1704.9854	1704.9873	$(y_{15}-1)^{4+}$	-1.1026
56	448.0163	1786.0063	1786.0068	$(b_{16}-H_2O)^{4+}$	-0.2800
57	596.3427	1786.0063	1786.0068	$(b_{16}-H_2O)^{3+}$	-0.2800
58	601.6911	1802.0515	1802.0526	$(z_{16}-1)^{3+}$	-0.6104
59	451.7720	1803.0591	1803.0604	$(z_{16})^{4+}$	-0.7210
60	602.0273	1803.0600	1803.0604	$(z_{16})^{3+}$	-0.2218
61	602.3464	1804.0175	1804.0168	$(b_{16})^{3+}$	0.3769
62	903.0161	1804.0176	1804.0168	$(b_{16})^{2+}$	0.4324
63	455.7768	1819.0779	1819.0792	$(y_{16})^{4+}$	-0.6954
64	607.3673	1819.0802	1819.0792	$(y_{16})^{3+}$	0.5690
65	911.0130	1820.0115	1820.0350	$(c_{16}-1)^{2+}$	-12.9118
66	462.5227	1846.0616	1846.0663	$(x_{16}+1)^{4+}$	-2.5216
67	616.3620	1846.0642	1846.0663	$(x_{16}+1)^{3+}$	-1.1132
68	943.5451	1885.0757	1885.0752	$(b_{17}-H_2O)^{2+}$	0.2652
69	629.3654	1885.0742	1885.0752	$(b_{17}-H_2O)^{3+}$	-0.5305
70	476.2750	1901.0707	1901.0696	$(b_{17}-2)^{4+}$	0.5786
71	476.7780	1903.0829	1903.0852	$(b_{17})^{4+}$	-1.2243
72	952.5499	1903.0853	1903.0852	$(b_{17})^{2+}$	0.0368
73	480.2829	1917.1024	1917.1033	$(z_{17})^{4+}$	-0.4851
74	640.3757	1918.1053	1918.1112	$(z_{17}+1)^{3+}$	-3.0759
75	484.2873	1933.1202	1933.1221	$(y_{17})_{4+}$	-0.9803
76	490.7824	1959.1004	1959.1014	$(x_{17})^{4+}$	-0.4900
77	1003.5765	2005.1384	2005.1407	$(a_{18}+1)^{2+}$	-1.1620
78	504.5361	2014.1155	2014.1178	$(b_{18}-H_2O)^{4+}$	-1.1419
79	672.3801	2014.1183	2014.1178	$(b_{18}-H_2O)^{3+}$	0.2482
80	1008.0663	2014.1181	2014.1178	$(b_{18}-H_2O)^{2+}$	0.1489
81	678.3826	2032.1261	2032.1278	$(b_{18})^{3+}$	-0.8464
82	509.0391	2032.1275	2032.1278	$(b_{18})^{4+}$	-0.1575
83	1017.0715	2032.1284	2032.1278	$(b_{18})^{2+}$	0.2854
84	521.0486	2080.1651	2080.1662	$(z_{18})^{4+}$	-0.5288
85	525.0538	2096.1862	2096.1854	$(y_{18})^{4+}$	0.3697
86	699.7362	2096.1868	2096.1854	$(y_{18})^{3+}$	0.6560
87	531.7999	2123.1707	2123.1725	$(x_{18}+1)^{4+}$	-0.8549
88	549.8058	2195.1943	2195.1936	$(z_{19})^{4+}$	0.3189
89	553.8093	2211.2082	2211.2124	$(y_{19})^{4+}$	-1.8836
90	575.5679	2298.2424	2298.2444	$(y_{20})^{4+}$	-0.8681
91	767.0886	2298.2440	2298.2444	$(y_{20})^{3+}$	-0.1719
92	582.3136	2325.2253	2325.2315	$(x_{20}+1)^{4+}$	-2.6600
93	603.5875	2410.3208	2410.3206	$(y_{21}-1)^{4+}$	0.0705

94	805.7750	2414.3033	2414.2772	$(b_{22}\text{-}H_2O)^{3+}$	10.8107
95	811.7741	2432.3006	2432.2872	$(b_{22})^{3+}$	5.4969
96	613.3351	2449.3114	2449.3135	$(c_{22})^{4+}$	-0.8696
97	817.4452	2449.3139	2449.3135	$(c_{22})^{3+}$	0.1511
98	624.8452	2495.3518	2495.3496	$(y_{22}\text{-}NH_3)^{4+}$	0.8816
99	832.7905	2495.3496	2495.3496	$(y_{22}\text{-}NH_3)^{3+}$	0.0000
100	513.4851	2562.3891	2562.3976	$(c_{23})^{5+}$	-3.3133
101	667.6242	2666.4676	2666.4616	$(y_{23}\text{-}2)^{4+}$	2.2502
102	534.5013	2667.4700	2667.4694	$(y_{23}\text{-}1)^{5+}$	0.2174
103	539.8986	2694.4568	2694.4565	$(x_{23})^{5+}$	0.1076
104	674.6220	2694.4589	2694.4565	$(x_{23})^{4+}$	0.8870
105	542.5051	2707.4893	2707.4887	$(y_{24}\text{-}H_2O)^{5+}$	0.2216
106	677.8803	2707.4920	2707.4887	$(y_{24}\text{-}H_2O)^{4+}$	1.2188
107	909.5072	2725.4999	2725.4987	$(y_{24})^{3+}$	0.4385
108	546.1073	2725.5000	2725.4987	$(y_{24})^{5+}$	0.4751
109	682.3824	2725.5005	2725.4987	$(y_{24})^{4+}$	0.6586
110	688.8863	2751.5160	2751.4780	$(x_{24})^{4+}$	13.8217
111	551.5038	2752.4825	2752.4858	$(x_{24}+1)^{5+}$	-1.1971
112	565.7105	2823.5163	2823.4996	$(y_{25}\text{-}NH_3)^{5+}$	5.9146
113	569.1124	2840.5257	2840.5256	$(y_{25})^{5+}$	0.0194
114	711.1394	2840.5287	2840.5256	$(y_{25})^{4+}$	1.0755
115	574.3076	2866.5018	2866.5049	$(x_{25})^{5+}$	-1.0849
116	591.3197	2951.5619	2951.5578	$(y_{26}\text{-}H_2O)^{5+}$	1.3891
117	738.8979	2951.5625	2951.5578	$(y_{26}\text{-}H_2O)^{4+}$	1.5924
118	600.3183	2996.5553	2996.5553	$(x_{26}+1)^{5+}$	-0.0084
119	771.6698	3082.6501	3082.6523	$(y_{27})^{4+}$	-0.7120
120	799.1825	3192.7009	3192.7004	$(y_{28}\text{-}H_2O)^{4+}$	0.1566
121	639.5475	3192.7012	3192.7004	$(y_{28}\text{-}H_2O)^{5+}$	0.2506
122	533.2913	3193.7042	3193.6844	$(y_{28}\text{-}NH_3)^{6+}$	6.1997
123	803.1870	3208.7188	3208.6947	$(y_{28}\text{-}2)^{4+}$	7.5108
124	810.1897	3236.7298	3236.6901	$(x_{28})^{4+}$	12.2533
125	825.9687	3299.8458	3299.8414	$(a_{30})^{4+}$	1.3349
126	554.9652	3323.7474	3323.7944	$(z_{29}+1)^{6+}$	-14.1405
127	557.4668	3338.7573	3338.8058	$(y_{29})^{6+}$	-14.5366
128	558.3084	3343.8069	3343.8545	$(c_{30}\text{-}1)^{6+}$	-14.2500
129	566.8041	3394.7807	3394.8195	$(y_{30}\text{-}1)^{6+}$	-11.4203
130	680.1742	3395.8346	3395.8273	$(y_{30})_{5+}$	2.1512
131	685.5697	3422.8124	3422.8144	$(x_{30}+1)^{5+}$	-0.5799
132	575.9809	3449.8419	3449.8384	$(y_{31}\text{-}NH_3)^{6+}$	1.0145
133	690.9771	3449.8489	3449.8384	$(y_{31}\text{-}NH_3)^{5+}$	3.0436
134	578.6497	3465.8548	3465.8566	$(y_{31}\text{-}1)^{6+}$	-0.5136

135	694.3801	3466.8643	3466.8644	$(y_{31})^{5+}$	-0.0303
136	867.7244	3466.8685	3466.8644	$(y_{31})^{4+}$	1.1812
137	583.1488	3492.8494	3492.8437	$(x_{31})^{6+}$	1.6405
138	699.5788	3492.8574	3492.8437	$(x_{31})^{5+}$	3.9309
139	588.6525	3525.8715	3525.9009	$(a_{32}\text{-}NH_3)^{6+}$	-8.3411
140	706.1854	3525.8907	3525.9009	$(a_{32}\text{-}NH3)^{5+}$	-2.8957
141	709.1883	3540.9054	3540.9113	$(a_{32}\text{-}2)^{5+}$	-1.6549
142	886.7391	3542.9274	3542.9269	$(a_{32})^{4+}$	0.1369
143	720.1917	3595.9220	3595.9228	$(y_{32}\text{-}H_2O)^{5+}$	-0.2225
144	600.4923	3596.9099	3596.9068	$(y_{32}\text{-}NH_3)^{6+}$	0.8591
145	603.3295	3613.9332	3613.9328	$(y_{32})^{6+}$	0.1065
146	904.4912	3613.9358	3613.9328	$(y_{32})^{4+}$	0.8260
147	723.7948	3613.9374	3613.9328	$(y_{32})^{5+}$	1.2687
148	607.6585	3639.9073	3639.9121	$(x_{32})^{6+}$	-1.3132
149	614.6692	3681.9718	3681.9903	$(b_{33}\text{-}NH_3)^{6+}$	-5.0163
150	619.3403	3710.0057	3709.9909	$(y_{33}\text{-}NH_3)^{6+}$	3.9973
151	619.3416	3710.9968	3710.9981	$(z_{33})^{6+}$	-0.3530
152	621.8474	3725.0408	3725.0012	$(y_{33}\text{-}2)^{6+}$	10.6255
153	746.4104	3727.0158	3727.0169	$(y_{33})^{5+}$	-0.2884
154	768.8246	3839.0864	3839.0931	$(y_{34}\text{-}1)^{5+}$	-1.7478
155	651.3563	3902.0939	3902.1071	$(c_{35})^{6+}$	-3.3930
156	794.8421	3969.1739	3969.1622	$(a_{36}\text{-}1)^{5+}$	2.9578
157	662.7018	3970.1670	3970.1700	$(a_{36})^{6+}$	-0.7519
158	993.5515	3970.1757	3970.1700	$(a_{36})^{4+}$	1.4395
159	795.2431	3971.1791	3971.1778	$(a_{36}+1)^{5+}$	0.3248
160	571.7485	3995.1888	3995.1942	$(y_{35}\text{-}1)^{7+}$	-1.3566
161	800.2412	3996.1695	3996.2020	$(y_{35})^{5+}$	-8.1440
162	667.0441	3996.2209	3996.2020	$(y_{35})^{6+}$	4.7182
163	1000.5490	3998.1668	3998.1649	$(b_{36})^{4+}$	0.4752
164	800.8404	3999.1657	3999.1727	$(b_{36}+1)^{5+}$	-1.7579
165	575.6056	4022.1880	4022.1813	$(x_{35})^{7+}$	1.6633
166	579.6089	4050.2111	4050.1967	$(a_{37}\text{-}NH_3)^{7+}$	3.5455
167	676.0432	4050.2154	4050.1967	$(a_{37}\text{-}NH_3)^{6+}$	4.6072
168	678.7180	4066.2641	4066.2149	$(a_{37}\text{-}1)^{6+}$	12.0948
169	678.8780	4067.2243	4067.2227	$(a_{37})^{6+}$	0.3823
170	814.6529	4068.2283	4068.2306	$(a_{37}+1)^{5+}$	-0.5580
171	685.5444	4107.2225	4107.2340	$(z_{36}\text{-}1)^{6+}$	-2.8072
172	587.8989	4108.2415	4108.2419	$(z_{36})^{7+}$	-0.0876
173	688.3842	4124.2613	4124.2606	$(y_{36})^{6+}$	0.1637
174	692.7163	4150.2515	4150.2399	$(x_{36})^{6+}$	2.7974
175	594.0427	4151.2477	4151.2477	$(x_{36}+1)^{7+}$	-0.0036

176	699.7144	4192.2429	4192.2704	$(b_{38})^{6+}$	-6.5645
177	702.3839	4208.2595	4208.2886	$(c_{38}-1)^{6+}$	-6.9268
178	706.7232	4234.2956	4234.3092	$(y_{37}-H_2O)^{6+}$	-3.2095
179	608.4803	4252.3111	4252.3192	$(y_{37})^{7+}$	-1.9060
180	851.4706	4252.3165	4252.3192	$(y_{37})^{5+}$	-0.6361
181	709.7279	4252.3237	4252.3192	$(y_{37})^{6+}$	1.0571
182	857.0696	4280.3107	4280.3103	$(a_{39}+1)^{5+}$	0.1005
183	612.6232	4281.3113	4281.3181	$(a_{39}+2)^{7+}$	-1.5883
184	715.8889	4289.2889	4289.2873	$(b_{39}-H_2O)^{6+}$	0.3730
185	858.8622	4289.2843	4289.2873	$(b_{39}-H_2O)^{5+}$	-0.6994
186	616.1971	4306.3287	4306.2895	$(b_{39}-1)^{7+}$	9.1030
187	862.4686	4307.3065	4307.2974	$(b_{39})^{5+}$	2.1220
188	871.2717	4351.3220	4351.3274	$(z_{38})^{5+}$	-1.2364
189	622.6268	4351.3365	4351.3274	$(z_{38})^{7+}$	2.0959
190	874.2712	4366.3369	4366.3383	$(y_{38}-2)^{5+}$	-0.3252
191	728.8984	4367.3465	4367.3461	$(y_{38})^{6+}$	0.0813
192	732.9024	4391.3706	4391.3098	$(x_{38}-2)^{6+}$	13.8455
193	733.2271	4393.3192	4393.3254	$(x_{38})^{6+}$	-1.4135
194	628.6250	4393.3242	4393.3254	$(x_{38})^{7+}$	-0.2754
195	879.6834	4393.3807	4393.3254	$(x_{38})^{5+}$	12.5850
196	735.7286	4408.3282	4408.3689	$(a_{40}+1)^{6+}$	-9.2211
197	740.2370	4435.3786	4435.3559	$(b_{40})^{6+}$	5.1089
198	636.2056	4446.3882	4446.3889	$(y_{39}-H_2O)^{7+}$	-0.1574
199	742.0705	4446.3794	4446.3889	$(y_{39}-H_2O)^{6+}$	-2.1366
200	743.2398	4453.3949	4453.3898	$(c_{40}+1)^{6+}$	1.1452
201	637.3511	4454.4065	4454.3976	$(c_{40}+2)^{7+}$	1.9980
202	638.4918	4462.3919	4462.3833	$(y_{39}-2)^{7+}$	1.9272
203	893.6841	4463.3840	4463.3911	$(y_{39}-2)^{5+}$	-1.5862
204	744.9057	4463.3908	4463.3911	$(y_{39}-1)^{6+}$	-0.0627
205	754.0786	4518.4277	4518.3926	$(a_{41}-NH_3)^{6+}$	7.7682
206	913.0968	4560.4477	4560.4438	$(y_{40}-1)^{5+}$	0.8464
207	652.5003	4560.4509	4560.4438	$(y_{40}-1)^{7+}$	1.5481
208	789.5994	4731.5530	4731.5572	$(y_{42})^{6+}$	-0.8845
209	798.9324	4787.5508	4787.5783	$(a_{43}-NH_3)^{6+}$	-5.7440
210	692.8077	4842.6029	4842.5898	$(y_{43}-H_2O)^{7+}$	2.7052
211	808.2729	4843.5938	4843.5738	$(y_{43}-NH_3)^{6+}$	4.1292
212	810.9403	4859.5947	4859.5919	$(y_{43}-1)^{6+}$	0.5659
213	811.2746	4861.6008	4861.6076	$(y_{43}+1)^{6+}$	-1.3987
214	820.7903	4918.6979	4918.6967	$(a_{44}+1)^{6+}$	0.2521
215	713.6782	4988.6962	4988.6947	$(y_{44})^{7+}$	0.2937
216	685.0026	5471.9627	5471.9514	$(y_{48}-1)^{8+}$	2.0559

217	696.3855	5563.0256	5563.0612	$(a_{50}+1)^{9+}$	-6.4066
218	736.6567	5885.1951	5885.2027	$(y_{52})^{8+}$	-1.2888
219	753.4139	6019.2526	6019.2455	$(a_{54})^{8+}$	1.1771
220	766.9225	6127.3202	6127.3293	$(y_{54})^{8+}$	-1.4909
221	686.1546	6166.3261	6166.3220	$(c_{55}+1)^{9+}$	0.6649
222	691.1579	6211.3559	6211.3510	$(y_{55}-NH_3)^{9+}$	0.7889
223	692.9365	6227.3631	6227.3692	$(y_{55}-1)^{9+}$	-0.9779
224	779.4281	6227.3663	6227.3692	$(y_{55}-1)^{8+}$	-0.4641
225	703.8272	6325.3794	6325.3939	$(y_{56}-H_2O)^{9+}$	-2.2923
226	704.4972	6331.4091	6331.3778	$(b_{57}-NH_3)^{9+}$	4.9436
227	793.8083	6342.4037	6342.3961	$(y_{56}-1)^{8+}$	1.1936
228	705.8305	6343.4091	6343.4040	$(y_{56})^{9+}$	0.8111
229	705.8305	6343.4091	6343.4040	$(y_{56})^{9+}$	0.8111
230	637.6519	6366.4117	6366.4381	$(c_{57}+1)^{10+}$	-4.1467
231	708.4972	6367.4097	6367.4459	$(c_{57}+2)^{9+}$	-5.6852
232	713.5014	6412.4470	6412.4260	$(y_{57}-H_2O)^{9+}$	3.2749
233	715.3919	6429.4614	6429.4282	$(y_{57}-1)9+$	5.1700
234	811.1894	6481.4573	6481.4651	$(c_{58}+1)^{8+}$	-1.2034
235	814.6917	6509.4754	6509.4543	$(z_{58}-2)^{8+}$	3.2414
236	651.9553	6509.4804	6509.4543	$(z_{58}-2)^{10+}$	4.0096
237	931.0763	6510.4799	6510.4622	$(z_{58}-1)^{7+}$	2.7187
238	724.5062	6511.4869	6511.4700	$(z_{58})^{9+}$	2.5985
239	933.4982	6527.4363	6527.4887	$(y_{58})_{9+}$	-8.0345
240	816.9437	6527.4918	6527.4887	$(y_{58})^{8+}$	0.4680
241	653.7569	6527.4964	6527.4887	$(y_{58})^{10+}$	1.1727
242	726.2849	6527.4982	6527.4887	$(y_{58})^{9+}$	1.4485
243	830.8229	6638.5270	6638.5209	$(y_{59}-H_2O)^{8+}$	0.9189
244	738.6210	6638.5232	6638.5209	$(y_{59}-H2O)^{9+}$	0.3465
245	664.8606	6638.5329	6638.5209	$(y_{59}-H_2O)^{10+}$	1.8076
246	751.4075	6753.6024	6753.5836	$(y_{60}-2)^{9+}$	2.7837
247	751.8513	6757.5961	6757.5637	$(c_{60})^{9+}$	4.7946
248	651.2827	8453.5810	8453.5475	$(x_{75}-1)^{13+}$	3.9628
249	705.5562	8454.5875	8454.5553	$(x_{75})^{12+}$	3.8039
250	772.3337	8484.5905	8484.5845	$(b_{75})^{11+}$	0.7025
251	777.5195	8541.6343	8541.6056	$(M-H_2O)^{11+}$	3.3630
252	712.8094	8541.6258	8541.6056	$(M-H_2O)^{12+}$	2.3678
253	658.0558	8541.6306	8541.6056	$(M-H_2O)^{13+}$	2.9298